Sentinel-3 Validation for Water Resources Protection

Report to the
WATER RESEARCH COMMISSION

by

MARK WILLIAM MATTHEWS[1,2]
JEREMY ALAN KRAVITZ[2]

[1]CyanoLakes (Pty) Ltd
[2]University of Cape Town (UCT)

WRC Report No 2518/1/19
ISBN 978-0-6392-0054-5

June 2019

Obtainable from

Water Research Commission

Private Bag X03

GEZINA, 0031

orders@wrc.org.za or download from www.wrc.org.za

EXECUTIVE SUMMARY

BACKGROUND

The “Sentinel-3 validation for water resources protection”, hereafter referred to as S3VAL, project aimed to provide measurements that support the quantitative calibration and validation (cal./val.) of the satellite remote sensing Sentinel-3 Ocean and Land Colour Instrument (OLCI) for water quality monitoring applications in water bodies and near-coastal waters of South Africa. The Sentinel-3A satellite was launched on 16 February 2016 and when fully operational will provide an unprecedented ability to observe the earth’s land and water surfaces for environmental applications. Sentinel-3A is the follow-on mission from the successful Envisat mission, which unexpectedly ended in April 2012. The Envisat satellite carried the Medium Resolution Imaging Spectrometer (MERIS) sensor which was successfully used for near real-time monitoring of eutrophication (nutrient enrichment), harmful algal blooms (HABs) and cyanobacteria (blue green algae) in inland and near-coastal marine waters of South Africa (e.g. Matthews & Bernard, 2015). The OLCI sensor is effectively a replacement sensor for MERIS (with several spectral and radiometric improvements) which will enable medium-resolution satellite-based monitoring applications for inland and coastal waters to continue from 2016 with a mission lifetime of seven years.

The S3VAL project builds on, compliments and supports several pre-existing initiatives and projects. The Sentinel-3 Validation Team (S3VT) organised by the European Space Agency (ESA) and EUMETSAT is tasked with reporting on the instrument performance during the commissioning phase (first approx. 6 months) of the Sentinel-3A OLCI sensor (February to August 2016). The South African S3VT team is composed of researchers and scientists from CSIR, DAFF, UCT, CyanoLakes (Pty) Ltd and other institutions. The “Integration of earth observation into the national eutrophication monitoring programme” (EONEMP) is a three-year project funded by the WRC aiming to utilise satellite-based monitoring of eutrophication, cyanobacteria and algal blooms to enhance the current programmes of the Department of Water and Sanitation. EONEMP includes field work and capacity building activities which closely complement those of S3VAL. S3VAL provides additional funds for capacity building, fieldwork and equipment expenditure that will be utilised to support and enhance the S3VT and EONEMP projects.

In summary, the S3VAL project focuses on the quantitative calibration and validation (cal./val.) of the OLCI sensor with a view to supporting water-related monitoring applications in South Africa to enhance protection and management of surface water resources.

RATIONALE

Satellite-based observations of water quality form a key component of current and ongoing monitoring programmes in South Africa aimed at the protection of our scarce and valuable surface water resources. However, in order for satellite-based observations to produce accurate information, it is necessary that data collected by satellite instruments be extensively validated with regards to their quantitative accuracy and quality. Such validation must be undertaken during satellite instrument commissioning, the time frame between launch and operational data provision, and further during the lifetime of the satellite mission.

The launch of Sentinel-3A in February 2016 was a watershed moment for satellite-based water-observing systems. The EONEMP project, and similar global water quality observation initiatives (e.g. led by the Group on Earth Observations), are largely reliant on the success of the OLCI mission for providing systematic observations of inland water bodies. This is because the OLCI instrument is ideally suited for water observations due to its precise radiometric, spectral, spatial and temporal instrument characteristics. The Sentinel-3A mission will consist of at least three identical satellite payloads providing continuous data over a minimum 20-year period; this long-term operational capability represents a significant opportunity and substantial return on South African investment in validation and mission exploitation.

The S3VAL project will contribute towards the development and production of accurate and validated products from OLCI for South African inland and coastal waters. The need for accurate and validated products for assessing water quality in South Africa is supported by previous WRC reports. The S3VAL project and related activities are aimed at ensuring that South Africa will reap the benefits of new satellite technology for our own economic, environmental and social needs. This will result in improved confidence and uptake of satellite-derived products in South African programmes; capacity building in an area of international skill scarcity; and utilization and development of South African technology for satellite validation and product development.

OBJECTIVES AND AIMS

The project has the following four aims:

AIM 1

To validate measurements of water colour (radiometry) and geophysical variables from the Sentinel-3A OLCI during instrument commissioning and afterwards

AIM 2

To collect high quality datasets from locally-developed, autonomous moored platforms (Buoy) to be used for validation of satellite-based measurements and development and testing of geophysical retrieval algorithms

AIM 3

To build human capacity and expertise in water remote sensing to meet the demands of the private, public and research sectors

AIM 4

To assess the data quality, absolute radiometric errors and the performance of standard atmospheric correction procedures of Sentinel-3A OLCI

METHODOLOGY

Data required for cal./val. of the Sentinel-3A was collected during the instrument commissioning phase and afterwards in 2016 and 2017 through four dedicated field campaigns. The data collected included high resolution measurements of the water colour (radiometry) and associated inherent optical properties including the absorption and scattering coefficients; atmospheric variables (e.g. aerosol optical thickness); geophysical parameters used to asses water quality including pigment chlorophyll-a; phytoplankton identification and counts; and ancillary data. An autonomous Buoy equipped with a variety of instrumentation was deployed for a period of three months and used to collect continuous measurements of the light field (upwelling irradiance and downwelling radiance) and various variables used for validation. Data from the Sentinel-3 OLCI sensor was acquired during the commission phase from the S3VT and afterwards from EUMETSAT. These were processed utilising open source tools where applicable (Sentinel-3 toolbox).

Matchups of simultaneously acquired OLCI data and in situ reference measurements of chl-a and water leaving reflectance were used to confirm the sensor performance and assess the performance of various chl-a models applied to OLCI. Reference reflectance measurements were modelled to top of atmosphere to assess the relative spectral and radiometric performance of OLCI. Several atmospheric correction techniques were applied to OLCI data and compered to reference field measurements. This included full atmospheric corrections deriving the water leaving reflectance and partial atmospheric corrections deriving top of atmosphere and intermediate products.

RESULTS

Aim 1

In situ reference datasets consisting of radiometric and biogeophysical measurements collected at four reservoirs of strategic importance in central Gauteng indicated significant impairment by cyanobacteria blooms and eutrophication, evidenced by high chlorophyll-a concentrations and cyanobacteria cell counts. Retrieval of biogeophysical variables (chl-a) from OLCI was feasible using models applied with partial atmospheric corrections, in particular the MPH algorithm with Rayleigh corrected reflectance. Conventional retrieval algorithms however failed. Results indicated that improved atmospheric corrections were needed before bio-optical models could be confidently applied with water leaving reflectance from OLCI in small eutrophic water bodies.

Aim 2

Time series measurements of water leaving reflectance and biogeophysical variables collected over a three month period by the autonomous Buoy at Roodeplaat Dam greatly increased the number of useable reference measurements for cal./val. of OLCI. The data compared closely to in situ reference measurements made by hand. It also demonstrated how autonomous technology with radiometers can effectively be used for providing short-term (hourly) and long-term (monthly) time series that provide significant insights into phytoplankton variability. The Bouy proved to be a reliable method for collecting ongoing radiometric data for validation, and demonstrated the utility of autonomous technology for estimating chl-a and other in-water bio-physical parameters. This study confirm the investment into locally developed platforms yields significant returns for satellite cal./val. activities.

Aim 3

The involvement of three students in the project has provided significant opportunities for skills transfer and capacity building to meet the needs of industry, government and academia. Effective collaboration between the project partners facilitated increased capacity building and learning opportunities for the students. Exhibition of the project results at local and international conferences and meetings (including the S3VT) has confirmed South Africa as a serious contributor to, and user of, satellite technologies through cal./val. activities.

Aim 4

Our assessment led to the finding that the unintended consequences of an increased viewing angle on OLCI relative to MERIS has led to significant drawbacks when sensing small (< 2 km) targets. This includes a larger ground sampling distance at edge of swath leading to

a significant increase in mixed duplicate pixels; a longer atmospheric path length increasing the appearance of stray light in the NIR bands; and a spatial offset of two to three pixels at high observation zenith angles. The result is a potential reduction in the number of viable sensing days, and increased likelihood of reduced quality for small targets. Despite these drawbacks, there was close comparison between OLCI TOA radiances and that modelled using reference measurements confirming that OLCIs radiometric and spectral performance was nominal, operating according to instrument specifications. This confirms OLCIs ability to resolve the spectral and radiometric characteristics of small eutrophic water body targets. An evaluation of several atmospheric corrections indicated that partial atmospheric corrections outperformed full atmospheric corrections when applied with bio-optical models. The performance of the atmospheric corrections tested for estimating water leaving reflectance were unsatisfactory, citing the need for the development alternative methods for use with OLCI in small inland water targets.

CONCLUSIONS

A thorough assessment of OLCI data has been performed during and after the commissioning phase of the instrument. The satellite is operating nominally and shows excellent potential for exploitation. However, for small targets, geolocation and high observation zenith angles remain a concern, and ways to correct for or avoid errors will need to be found. In situ data collected at four water bodies in central Gauteng provided data to validate the results of atmospheric corrections. Initial results indicate that due to the extreme optical nature of the atmosphere and water bodies in the region, full atmospheric corrections are very difficult to perform successfully, highlighting the need for specialised or improved atmospheric corrections for OLCI. Partial atmospheric corrections were superior for the application of models using bands in the green and red spectral region. The MPH algorithm with Rayleigh corrected reflectance was the best performing method for estimating chl-a from OCLI when compared to alternative models. The autonomous Buoy provided invaluable high-resolution time series of high quality radiometric and geophysical measurements that were of considerable value for cal./val. efforts. Validation of OLCI provides compelling evidence that it has the capability to provide accurate information for protection of water resources from the twin risks of cyanobacteria blooms and eutrophication in South Africa’s bulk storage surface water resources.

RECOMMENDATIONS FOR FUTURE RESEARCH

The following recommendations are based on the outcomes of this research:

- The Sentinel-3 mission can with confidence be utilized for inland water remote sensing applications owning to its high spectral and radiometric quality that accurately characterises inland water targets
- Cal./val. should be undertaken for the remaining Sentinel-3B and -3C missions scheduled for launch in 2018 and 2019/20 respectively
- Given its performance, the MPH algorithm applied to BRR corrected data should be utilised in operational systems for chl-a estimation
- Continuous development and deployment of locally-developed buoys equipped with radiometers would substantiate cal./val. efforts and add significant concomitant value to satellite-based monitoring efforts by providing high quality data for validation, for the development of atmospheric corrections methods, and for short-term (daily) and long-term (monthly) monitoring of phytoplankton variability
- Work should intensify to test and develop a robust atmospheric correction procedure that is applicable in inland waters where complex effects from high aerosol loading, adjacency effects (stray light) and water variability interact

ACKNOWLEDGEMENTS

Acknowledgement is due to Derek Griffith at CSRI DPSS for contributions to the sections on atmospheric modelling and measurements, and to Stewart Bernard at CSIR NRE for providing use of the autonomous Buoy and contributions from related CSIR research projects. The authors would like to thank the Reference Group of the WRC Project K5/2518 for the assistance and the constructive discussions during the duration of the project: Shafick Adams, Stewart Bernard, Derek Griffith, and Chris Moseki. Thanks go to Department of Water and Sanitation Resource Quality Information Services staff: Michael Silberbauer, Paul Botes, Sazi Mthembu, Elna Vermaak, Solomon Mahladisha, Gerhard Cilliers, Brendan Hohls, and Elna Portwig and others who assisted with data collection, lab analysis and servicing of the autonomous Buoy. Thanks to CSIR Optronics Hein Swart and Peter Bosscha for deployment and servicing of the Buoy. Russell Main and Renaud Mathieu at CSIR NRE are thanked for use of the ASD instrument. Thanks to other students involved who assisted with data collection: Kenilwe Hlahane and Zimbini Faniso. Annelie Swanepoel and Rand Water are gratefully acknowledged for phytoplankton identification and counts.

This page was intentionally left empty

TABLE OF CONTENTS

LIST OF FIGURES

LIST OF TABLES

LIST OF ABBREVIATIONS

BRR	Bottom of Rayleigh reflectance
CDOM	Coloured Dissolved Organic Matter
Chl-*a*	Chlorophyll-*a*
C2RCC	Case 2 Regional Coast Colour Processor
DWS	Department of Water and Sanitation
FLH	Fluorescent Line Height
MCI	Maximum Chlorophyll Index
MERIS	Medium Resolution Imaging Spectrometer
MODIS	Moderate Resolution Imaging Spectrometer
MSI	Multi Spectral Imager
OLCI	Ocean and Land Colour Instrument
OZA	Observation Zenith Angle
RQIS	Resource Quality and Information Services
R_{RS}	Remote Sensing Reflectance
6SV1	Second simulation of a Satellite Signal in the Solar Spectrum, version 1

This page was intentionally left blank

1 INTRODUCTION AND OBJECTIVES

1.1 Context and motivation

Satellite-based observations of water quality form a key component of current and ongoing monitoring programs in South Africa aimed at the protection of our scarce and valuable surface water resources, including the WRC funded EONEMP project (K5/2458), and the Operation Phakisa Oceans and Coastal Information Management System. In order for satellite-based observations to produce accurate information, it is necessary that data collected by satellite instruments be extensively validated with regards to their quantitative accuracy and quality. Such validation must be undertaken during satellite instrument commissioning, the time frame between launch and operational data provision, and further undertaken during the mission lifetime. The Sentinel-3 Validation for Water Resources Protection (S3VAL) project concerns the validation of the OLCI instrument for monitoring of South African inland waters through fieldwork during and after the launch of Sentinel-3A satellite in order to provide validated information for decision making in downstream applications.

1.2 The Copernicus programme and Sentinel-3

Copernicus is the European Union's programme for earth observation which incorporates both ground (in situ) and satellite monitoring previously known as Global Monitoring for Environment and Security (GMES) (www.copernicus.eu). Copernicus aims to build capacity for observing the earth by collecting data from ground- and earth-based sensors to improve decision making and quality of life. The data policy provides open and free access to all users. The satellite component owned and managed by the European Commission under the European Space Agency consists of a series of six satellite missions called the Sentinels. Each of the Sentinels have a specific monitoring mission that covers the atmosphere, ocean, land, climate and emergency and security needs. This provides a vast amount of data for earth observation and monitoring.

The Sentinel-3 satellite mission is part of the European Commission's Copernicus programme for earth observation solutions from satellite. The Sentinel-3 platform is equipped with instruments that will measure the colour, temperature and height of ocean and land surfaces with high accuracy for environmental monitoring and climate change applications (https://sentinel.esa.int/web/sentinel/missions/sentinel-3). The first Sentinel-3 satellite, Sentinel-3A was successfully launched on 16 February 2016. A constellation of Sentinel-3 satellites, named Sentinel-3B and Sentinel-3C, are planned for subsequent years which will increase data coverage to a global daily latency, and ensure operational capability to at least year 2030. This will provide an unprecedented ability to measure environmental changes

occurring on the earth's surface, and the quality of inland and coastal waters. The sensors on board Sentinel-3 are of particular use and interest due to its ability to detect and provide information for small water bodies.

1.3 The Ocean and Land Colour Instrument

The Ocean and Land Colour Instrument (OLCI) on board Sentinel-3 is a heritage sensor following on from the Medium Resolution Imaging Spectrometer (MERIS) on-board the Envisat platform. Envisat was operational from 2002 until April 2012, which exceeded its mission lifetime of seven years. MERIS provided an unprecedented capability to monitor coastal and inland water systems from 2002 until 2012. MERIS contained bands particularly suited to capturing chlorophyll-a fluorescence and the red-edge. The spectral bands are sufficient to discriminate between cyanobacteria and algae species, and derive a quantitative estimate of chlorophyll-a, the primary pigment used for nutrient enrichment (eutrophication) assessment, thus MERIS was very successfully in its ability to monitor smaller and more complex water targets (Matthews et al., 2014; Palmer et al., 2014; Binding et al., 2011).

OLCI, like its predecessor MERIS, has ideal spatial, spectral and radiometric characteristic that enable quantitative, routine estimates of water quality variables for water bodies larger than 1 km^2 (see Table 1 for instrument characteristics). Given that dark water targets have demanding requirements when measuring from space, conventional land and RGB type sensors (e.g. SPOT, Landsat, etc.) do not meet the minimum radiometric and spectral requirements for many water-related applications (particularly quantitative cyanobacteria and chlorophyll-a detection). The failure of MERIS halted many of the operational water quality applications that relied upon it. Thus OLCI is a unique and vital sensor that will enable many critical water applications to continue from where MERIS left off.

Table 1: Sentinel-3A OLCI instrument characteristics

Swath / image width	1440 km
Ground sampling distance / pixel size	300 m
Spectral resolution	21 bands at 1.25 nm resolution (MERIS + 5 new bands)
Radiometric accuracy	< 2% for 400-900 nm and < 5% for wavebands > 900 nm. 0.1% stability over each orbit and 0.5% relative accuracy.
Radiometric resolution	< 0.03 W m^{-2} sr^{-1} mm^{-1}

OLCI has a number of improvements when compared to MERIS including an increase from 15 to 21 spectral bands, improved SNR, tilted cameras for mitigation of sun-glint, global spatial resolution of 300 m at full resolution, and improved coverage. The OLCI bandwidths are provided in Table 2. OLCI thus provides an essential information source for eutrophication and associated toxic algal blooms in water resources.

Table 2: OLCI band characteristics (new bands in bold).

Band	λ Center	Width	L_{min}	L_{ref}	L_{sat}	OLCI
#	nm	nm	W/(m^2.sr.μm)	W/(m^2.sr.μm)	W/(m^2.sr.μm)	SNR@FR
Oa1	**400**	**15**	**21.6**	**62.95**	**413.5**	**2188**
Oa2	412.5	10	25.93	74.14	501.3	2061
Oa3	442.5	10	23.96	65.61	466.1	1811
Oa4	490	10	19.78	51.21	483.3	1541
Oa5	510	10	17.45	44.39	449.6	1488
Oa6	560	10	12.73	31.49	524.5	1280
Oa7	620	10	8.86	21.14	397.9	997
Oa8	665	10	7.12	16.38	364.9	883
Oa9	**673.75**	**7.5**	**6.87**	**15.7**	**443.1**	**707**
Oa10	681.25	7.5	6.65	15.11	350.3	745
Oa11	708.75	10	5.66	12.73	332.4	785
Oa12	753.75	7.5	4.7	10.33	377.7	605
Oa13	761.25	2.5	2.53	6.09	369.5	232
Oa14	**764.375**	**3.75**	**3**	**7.13**	**373.4**	**305**
Oa15	**767.5**	**2.5**	**3.27**	**7.58**	**250**	**330**
Oa16	**778.75**	**15**	**4.22**	**9.18**	**277.5**	**812**
Oa17	865	20	2.88	6.17	229.5	666
Oa18	885	10	2.8	6	281	395
Oa19	900	10	2.05	4.73	237.6	308
Oa20	**940**	**20**	**0.94**	**2.39**	**171.7**	**203**
Oa21	**1020**	**40**	**1.81**	**3.86**	**163.7**	**152**

1.4 Cyanobacteria and eutrophication: twin risks to South Africa's water resources

Over recent decades the natural ageing, or eutrophication, of inland water bodies have been greatly accelerated by anthropogenic influence in South Africa (Smith et al., 2014; Van Ginkel, 2008). The anthropogenic influence on eutrophication in South Africa is widespread due to poor infrastructure and staffing policies, budget issues, and national scarcity in personnel trained in limnologic sciences. Urban runoff such as mistreated effluent from populated regions and waste from industrial processes empty into sewers and rivers, eventually transporting hazardous chemicals to inland reservoirs (Nyenje et al., 2010; Le Roux et al., 2012). Drainage of pesticides and fertilizers from the burgeoning agricultural industry also find their way to

inland water reservoirs contributing to nutrient enrichment (Walmsley, 2000). Effects from climate change also has the potential to exacerbate nutrient enrichment and increase water temperatures (Jeppeson et al., 2014). The implications and ramifications of reduced water quality and an increasing predominance of eutrophication in South Africa have been highlighted in recent years (Harding, 2015; Oberholster and Ashton, 2008; Van Ginkel, 2011; Van Ginkel et al., 2004), as well as reviews emphasizing the necessity for improved management practices (Van Ginkel, 2012). The common consensus is that South Africa's already limited freshwater resources will become further reduced as water quality degradation and eutrophication continues.

Eutrophication is a trophic classification defined as an enrichment of nutrients in a water body that results in excessive algal and aquatic macrophyte growth. A water body can be classified as oligotrophic, mesotrophic, eutrophic, or hypertrophic depending on the level of nutrient enrichment and algal biomass. The Department of Water Affairs and Forestry South Africa classifies a water body as eutrophic when mean chlorophyll-a values range between 20-30 μg/l or total phosphorous levels range between 0.047-0.130 mg/l while hypertrophy exists when chlorophyll-a exceeds 30 μg/l or total phosphorous exceeds 0.130 mg/l (DWAF, 2002). A Department of Water and Sanitation report in 2008 found that of the water bodies under their water quality monitoring program, 42% were classified as eutrophic (DWAF, 2008). Increased nutrient holdings have been linked to harmful algal growth such as toxic Cyanobacteria (Carvalho et al., 2013; Schindler et al., 2008). Cyanobacteria's high affinity for N and P gives them a competitive advantage during short bouts of enrichment (Paerl et al., 2011).

While the growth rate of Cyanobacteria is quite low compared to other phytoplankton groups, they tend to dominate in light limited conditions due to their capacity for buoyancy regulation and their high affinity for light (Mur & Schreurs, 1995). Warming water temperatures also create ripe conditions for Cyanobacterial growth with maximal growth rates above 25°C which are higher than other bloom forming phytoplankton (Robarts & Zohary, 1987; Chorus and Bartram, 1999). As we see warming temperatures from a changing climate, we are starting to see a shift towards more Cyanobacteria dominated waters (Mooij et al., 2007; Joehnk et al., 2008). In South Africa, *Microcystis* spp. is the dominant bloom-forming cyanobacteria species present (Harding & Paxton, 2001; Downing & Van Ginkel, 2003). In periods of low wind and stagnation, stratified water columns provide conditions for the creation of dense cyanobacterial surface blooms, known as scums, further decreasing light availability for other phytoplankton groups below.

The presence of Cyanobacteria poses significant health risks (Falconer & Humpage, 2006) mainly due to the production of various toxins (Bláha et al., 2009). While deaths from cyanobacteria poisoning of livestock and wildlife have been reported (Oberholster et al., 2009), human fatalities are very rare. However, long-term chronic exposure to cyanotoxins in domestic water poses a serious threat (Oberholster & Ashton, 2008). The eutrophication problem places an economic burden on South Africa affecting costs associated with recreational activity, industry, property value, and agriculture. Not to mention the costly measures associated with remediation of the issue pertaining to improved management and monitoring practices, chemical and biological methods for hindering toxic algal blooms and nuisance floating aquatic macrophytes, and improved infrastructure. In Harding (2015) it is noted that the South African government will require upwards of $60 billion to overhaul a failing infrastructure and just a 1% overall decrease in water quality would have large economic ramifications including a 5% increase in government spending.

South Africa has close to 600 large reservoirs in addition to over 150,000 smaller reservoirs and farm dams with a high percentage of them being artificial. Government programs such as the National Eutrophication Monitoring Program (NEMP) monitor conditions conducive to eutrophication events which can lead to the production of potentially toxic algal species. While the effort has had positive outcomes, initiatives such as these are limited in its scope and application to costly and time-consuming point source studies and are generally restricted to a handful of reservoirs. Recent advancements in the remote sensing of coastal, estuarine, and inland water bodies have provided a positive outlook for improved monitoring efforts (Palmer et al., 2015).

1.5 Protection of water resources using Sentinel-3

The unique spectral, radiometric and spatial characteristics of OLCI make it the optimal satellite sensor for water applications for water bodies larger than approx. 1 km^2. In particular, the spectral bands are sufficient to discriminate between cyanobacteria and algae species, and derive a quantitative estimate of chlorophyll-a, the primary pigment used for nutrient enrichment (eutrophication) assessment. Thus, OLCI provides an essential information source for the twin risks of cyanobacteria blooms and eutrophication in water resources. Therefore, there is substantial motivation to develop suitably calibrated and validated products from OLCI for these risks. Given the consistency (frequency), spatial coverage and accuracy of OLCI, it provides an opportunity for monitoring these risks (in conjunction with in situ measurements used for cal./val.) that surpasses traditional methods of monitoring, and resultantly has high economic and societal value.

In addition, it is essential that OLCI data be reliability calibrated and validated at both top-of-atmosphere (TOA) and bottom-of-atmosphere (BOA). TOA measurements comprise of radiances measured in W m^{-2} sr^{-1} mm^{-1} as contained in the product Level 1 files. BOA products consist of water leaving reflectance after atmospheric correction (units sr^{-1}), as well as geophysical products such as chlorophyll-a and are contained in product Level 2 files. It is essential to characterize both the error at TOA related to the instrument measurements themselves, and errors in the derived products at BOA. This will improve confidence in the product quality level, in order to meet the minimum quality standards for various applications.

Aims and Objectives

The S3VAL project has the following aims and objectives:

1. To validate measurements of water colour (radiometry) and geophysical variables from the Sentinel-3 Ocean and Land Colour Instrument during the instrument commissioning phase and afterwards

2. To collect high quality datasets from locally developed, autonomous moored platforms to be used for validation of satellite-based measurements and development and testing of geophysical retrieval algorithms

3. To build human capacity / expertise in water remote sensing to meet the demands of the private, public and research sectors

4. To assess the data quality, absolute radiometric errors and the performance of standard atmospheric correction procedures of Sentinel-3 OLCI

2 DATA AND METHODS

2.1 Study sites

Four inland water reservoirs were visited between June 2016 and November 2017 (Figure 1). The Hartbeespoort, Roodeplaat, Bronkhorstspruit, and Vaal Dams are situated in the Gauteng Province of South Africa. A summary of basic catchment characteristics of the water impoundments can be found in Table 1.

Water from the dams are routinely used for the region's domestic water supply, irrigation and agriculture, as well for public recreation and water sports. The Gauteng Province is one of the most densely populated regions of South Africa, leading to large implications for cultural eutrophication within the local inland water reservoirs. All four dams regularly see chlorophyll-a concentrations that exceed the 30 µg/L thresholds to be classified as hypertrophic systems (Matthews, 2014; DWAF, 2002). It is not uncommon for concentrations of Chlorophyll-a in Hartbeespoort Dam to reach into the thousands (Harding, 2015) and for the water surface to reach hyper-scum conditions (Zohary, 1985). In both Hartbeespoort and Roodeplaat dam, cyanophyta, primarily M. aeruginosa, dominates the algal assemblage throughout the year with intermittent blooms of chlorophyta, chrysophyta, and cryptophyta that have been previously identified (Van Ginkel, 2007).

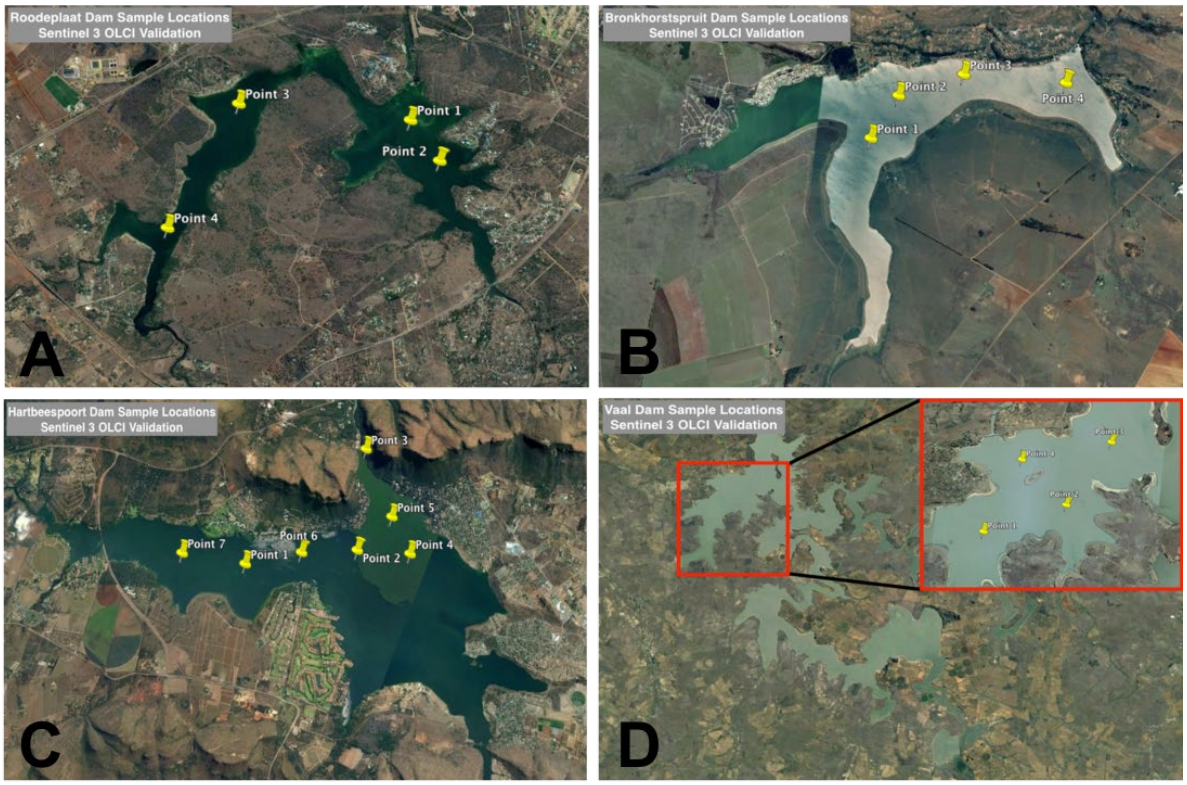

Figure 1: In situ sampling points. A) Roodeplaat Dam, B) Bronkhorstspruit Dam, C) Hartbeespoort Dam, D) Vaal Dam

Hartbeespoort Dam's growing popularity as a vacation destination has contributed to the expanding urbanization of the surrounding region along with multiple resort style hotels. The impoundment is a warm, monomictic lake which resides in a valley between the Magaliesberg and Witwatersberg mountain ranges. The main catchment also contains 16 sewage treatment works and numerous intensive farming works that threaten the reservoirs water quality due to effluent discharge (Van Ginkel, 2007). One of the main river inflows, the Crocodile River, supplies 90% of water inflow to Hartbeespoort Dam and 99% of its nutrient load (Scott et al., 1980). A floating invasive plant, *Eichhornia* crassipes, commonly known as water hyacinth, has been a particularly troublesome weed that has spread through many of South Africa's inland water systems (Cilliers, 1991; Coetzee and Hill, 2012). While sightings have occurred at the four dams under investigation, Hartbeespoort regularly sees large scale growths of the weed with dam coverage capable of exceeding 60% (Scott et al., 1980). Water hyacinth can severely diminish the economic value of the dams due to eliminating the capability for boat activity, water loss through evapotranspiration, clogging of damn inlets/outlets, and providing breeding ground for nuisance insects (Van Wyk and Van Wilgen, 2002). During periods of high water hyacinth growth, water clarity and quality improves as the aquatic plant takes up most of the nutrients in the impoundment, limiting the growth of harmful algae. Many chemical and biological controls have been utilize in attempt to suppress the problem with varying results (Cilliers, 1991; Byrne et al., 2010; Van Wyk and Wilgen, 2002).

The region surrounding Roodeplaat Dam is dominated by Highveld grassland, scrub covered middelveld ridges and bushveld with less urbanization than Hartbeespoort and part of the surrounding area designated as a Natural Reserve. Even though less industrialization exists, Roodeplaat is still identified as one the most eutrophic inland water bodies in South Africa under Hartbeespoort and Rietvlei (Toerien, Hyman, and Brewer, 1975). A large contributing factor for the degradation of the water quality in Roodeplaat is the secondary treated sewage that makes its way into the dam by way of the Pienaars river in the southwest region of the dam (Walmsley and Toerien, 1978). Two sewage treatment works are located in the catchment and discharge can reach up to 25% of total water inflow of the dam, also bringing in large amounts of inorganic nutrients (Walmsley et al., 1978). A higher nutrient load in the western part of the impoundment generally results in increased prevalence of cyanobacteria dominance in this region (Pieterse and Rohrbeck, 1990). The Resource Quality and Information Services (RQIS) as part of the Department of Water affairs have offices located adjacent to the reservoir on the northern side and allows easy access to the dam.

Table 3: Summary of major dam characteristics

Reservoir	Hartbeespoort	Roodeplaat	Bronkhorstspruit	Vaal
Location	25°43’30” S; 27°51’ E	23°58’ S; 27°43’ E	25°53’25” S; 28°24’43 E	26°54’11” S; 28°08’31 E
Altitude	1,162 m	1,314 m	1,429 m	1,486 m
Catchment area	4,144 km^2	668 km^2	1,263 km^2	37,100 km^2
Volume	195 x 10^6 m^3	41.9 x 10^4 m^3	58.5 x 10^6 m^3	2,330 x 10^6
Surface area	20 km^2	3.96 km^2	8.5 km^2	321.07 km^2
Max Depth	32.5 m	43 m	19.5 m	47 m
Mean Depth	9.6 m	10.6 m	6.8 m	22.5 m

Hartbeespoort and Roodeplaat dams are similar in their algal assemblage and IOP characteristics, however, Bronkhorstspruit dam differs in that it is generally dominated by diatoms and eukaryotic algae and contains the best water quality (Thirion, 2000). However, recent studies have shown chlorophyll-a concentration in Bronkhorstspruit to be quite high with average chlorophyll-a concentrations around 100 µg/L and an increase in the prevalence of cyanobacterium (Matthews, 2014). Bronkhorstspruit dam is located about 50 km east of Pretoria in the Gauteng Province and frequently sees high amounts of tourism during the summer season with moderate urbanization and development surrounding the dam.

While Hartbeespoort, Roodeplaat, and Bronkhorstspruit are all quite small dams with surface areas about 20 km^2 and below, Vaal Dam is by far the biggest with a surface area of roughly 320 km^2. The Vaal Dam resides on the southern edge of Gauteng Provence and is the dominant water supply for roughly 12 million people. It is the most important water source for the Gauteng and surrounding regions which rely on the dam for potable water. The dam is separated into an Upper, Middle, and Lower Water Management Area (WMA). The actual Vaal Dam sits in the Upper WMA and is heavily urbanized with high amounts of industry from coal and gold mining, creating high economic value (Chinyama et al., 2016). The dam is fed by the Vaal River from the northeast and the Wilge River from the southeast, covering both the middle and lower WMA’s. Over the years, the poorly treated effluent from the Upper WMA has been degrading the Vaal Dam’s water quality, creating conditions conducive for eutrophic to even hypertrophic states.

Table 4: GPS locations of sample points

Reservoir	Hartbeespoort	Roodeplaat	Bronkhorstspruit	Vaal
Point 1	25°45'18.0” S; 27°50'9.60" E	25°37'34.32" S; 28°22'18.48" E	25°54'12.10" S; 28°41' 6.53" E	26°54'58.65" S; 28°07' 03.3" E
Point 2	25°44'38.40" S; 27°51'25.20" E	25°37'49.44" S; 28°22'28.56" E	25°53'53.48" S; 28°41'27.74" E	26°54'11.1" S; 28°08' 31.1" E
Point 3	25°43'33.24" S; 27°50'54.96" E	25°37'33.7 " S; 28°21'00.5" E	53'47.90" S; 28°41'57.58" E	26°52'57.2" S; 28°09' 31.1" E
Point 4	25°53'37.5" S; 28°43'9.55" E	25°38'24.0" S; 28°20'37.2" E	25°53'37.5" S; 28°43'9.55" E	26°53'32.3" S; 28°07' 37.2" E
Point 5	25°44'10.4" S; 27°51'34.6" E			
Point 6	25°44'56.7" S; 27°50'48.4" E			
Point 7	25°45'30.0" S; 27°49'23.3" E			

Sample points for the four dams were arranged in areas in which the highest probability was for obtaining a clear water pixel not contaminated by the surrounding land. During the 2016 field campaigns, only two sample locations were used at the smaller Roodeplaat Dam, with surface and three-meter depths being sampled. Four locations were sampled per day at the larger Hartbeespoort and Bronkhorstspruit dams with only surface samples being collected. During the 2017 field campaign, four locations were sampled for surface water at all reservoirs with the inclusion of Vaal Dam. Sampling locations may have changed during different fieldwork campaigns due to environmental or logistical reasons, but total number of points were kept no greater than four. A summary of the major characteristics of the four dams and the locations of all in situ sample points can be seen in Table 3 and Table 4, respectively. Images of the dams showing locations of the sample points can be seen in Figure 1. Given the size of the dams, it is possibly only to obtain a few clear water pixels not contaminated by land. Hartbeespoort and Vaal are larger reservoirs and a greater number of clear pixels may be obtained; while Roodeplaat likely represents the smallest body of water that can be observed with OLCI, and therefore a test of an extreme case for observing small eutrophic waters. Sampling in Hartbeespoort was hampered in 2017 by the growth and proliferation of water hyacinth, which covered around 30% of the area of the reservoir making it impossible to sample certain points.

2.2 Biogeophysical and radiometric measurements

The validation of OLCI products consisted of biogeophysical data collected in-situ on the same day as Sentinel-3A overpasses with a time lag between overpass and collection no greater than four hours. Measurements for water quality, water clarity, and visual information on weather and water surface conditions were collected by small boat at each station. Water clarity was determined by Secchi disc method. The disc was lowered into the water until the black and white quadrants are just visible and the depth is recorded. This was performed twice and an average was taken as the final result. Water samples are collected by first rinsing a 25L black bucket three times with surface water followed by the actual collection of a surface water sample. The bucket is then sealed with a lid and vigorously shaken to allow adequate mixing of the sample. Various water quality parameters are then sub-sampled from the 25 L bucket. For chlorophyll-a and total suspended solids analysis (TSS), two well-rinsed 1 L bottles were used to collect water from the surface of the bucket, taking great care as to not disturb the phytoplankton assemblages and to minimize bubbles. Samples for phytoplankton identification and enumeration were collected in the same manner in a well-rinsed 100 ml bottle. Sample bottles were kept cold and in the dark until brought back to land in which they were placed in a -5°C refrigerator until analysis. Chlorophyll-a and TSS analysis took place no later than one day from collection. Samples for phytoplankton enumeration were preserved with formaldehyde until analysis by Rand Water. Time between collection and analysis for phytoplankton enumeration ranged between one and two months.

Samples for chl-a analysis were kept between 2 and 4°C and analysed on the same day of sampling or within 24 hrs. For each batch of samples, a duplicate and a blank were measured. The volume of the amount of sample filtered varied depending on the amount of phytoplankton present. Filtering volumes ranged between 100 to 500 ml with clearer waters requiring higher filter volumes. Samples were filtered onto Whatman GFF and placed into screw capped test tubes with ethanol solution to extract the pigments. Test tubes are heated and gently boiled and placed in the dark at room temperature until cooled. The extract was decanted and centrifuged and the concentration of chl-a and phaeopigments were determined by measuring the absorbance in a spectrophotometer, before and after acidification of the extract.

Measurements of total suspended solids (TSS) were performed gravimetrically. Previous to fieldwork sampling, Whatman GFF filters were rinsed with DI water to rinse filters of any particles prior to field sampling. Filters were then dried in an oven at 105°C for one hour and placed in the desiccator to cool until further use. Filters were then weighed for dry weight and recorded. Similar to the chl-a analysis, volume of sample filtered varied depending on particle load of the water sample. Ideally, at least 100 ml of sample was filtered, however, this ranged

between 50 and 300 ml depending on the particle load. Filters were rinsed with 20 ml of DI water previous to sample filtration. Filters were then oven dried at 105°C for at least two hours and placed into the desiccator to cool until being re-weighed. TSS was then calculated using equation 1 and reported in mg/L.

$$\text{TSS (mg/L)} = \frac{(A-B)x\ 1000}{C} \quad (1)$$

where, A is the weight of the filter and residue (mg), B is the weight of the filter (mg), and C is the volume in ml of sample filtered.

Phytoplankton samples for enumeration and identification were pressure deflated followed by homogenization at 1300 rpm for 15 seconds. Upon completion, 3 ml of sample was pipetted into a sedimentation chamber which was centrifuged for 10 minutes at 3500 rpm to allow algal cells to settle. Identification of phytoplankton genera was completed by identification keys and enumerated by use of an inverted light microscope. Concentration of algae genera were then reported in cells/ml of sample. For full details of enumeration methods see Swanepoel et al. (2008).

During field campaigns, radiometric data was collected concurrently with water samples using an ASD-FR Field Spectroradiometer 3 (Analytical Spectral Devices, Boulder, CO USA). Methods to derive remote sensing reflectance were derived from Mueller et al. (2003) and briefly described here. Measurements of a white Spectralon reflectance plaque with a known BRDF were used to normalize the uncalibrated radiance measurements for downwelling irradiance, $E_s(\lambda;\theta o)$. The plaque was held horizontally and exposed to the sun, free from any shading or reflections by equipment, the boat, or crew. Radiances of the plaque (S_g) were recorded using a viewing angle of $\theta = 40°$ away from the nadir and azimuthally away from the sun at $\phi = 135°$ and ten spectra were collected. Immediately following measurements of S_g, the radiometer was used to collect both water and sky radiance measurements, $L_{sfc}(\lambda,\theta,\varphi \in \Omega FOV;\theta 0)$ and $L_{sky}(\lambda,\theta sky,\varphi sky \in \Omega' FOV;\theta o)$ respectively. Measurements were performed using the same zenith and azimuthal viewing angles as the plaque and again, ten spectra were collected for each.

Measurements were collected on the sunny side of the boat and precautions were taken not to collect water measurements in recently disturbed water from the boat or where there was excessive surface roughness. Once completed, a dark offset reading was taken and the whole process was repeated three times with the mean of the spectra being used. Using equations

defined in Mueller et al. (2003), Remote Sensing Reflectance (R_{RS}) was calculated for each station using Water leaving radiance (L_w) and estimated downwelling irradiance (E_s):

$$R_{RS}(\lambda, \theta, \varphi \in \Omega_{FOV}; \theta_0) = \frac{L_w(\lambda, \theta, \varphi \in \Omega_{FOV}; \theta_0)}{E_S(\lambda; \theta_0)} \quad (2)$$

Data on atmospheric variables were also obtained coincident with satellite overpasses. Aerosol Optical Thickness (AOT) was measured at wavelengths of 400 nm, 500 nm, 675 nm, and 870 nm using a MicroTOPS II handheld sunphotometer. An additional optical thickness measurement at 936 nm is used to estimate the total water vapour column. In addition, an AERONET station located at CSIR Pretoria, South Africa (GPS: 25°45'25.2" S, 28°16'48" E) which houses a Cimel CE318 robotic sunphotometer was used to acquire atmospheric data on overpass dates where MicroTOPS II data was not available or as a reference.

2.3 Measurements from an autonomous Buoy

An autonomous Buoy developed by the Council for Scientific and Industrial Research (CSIR) was moored at Roodeplaat Dam for three months (between June and August 2016) to collect continuous radiometric measurements to be used for validation purposes (Figure 2). The radiometric payload consists of one Trios RAMSES ACC downwelling irradiance sensor and two Trios RAMSES ARC upwelling radiances sensors at 0.15 and 0.76 m depths. All radiometric sensors are directed at nadir. Other sensors include a Trios fluorometer measuring chlorophyll-a fluorescence, an ultrasonic anemometer, pitch and roll sensors, and a temperature sensor. The control operations for the Buoy system were set to collect measurements for all instrumentation in 5 minute bursts every 15 minutes and was battery powered, charged by two solar panels attached above the water surface. The data were transmitted via GSM telemetry for real-time data acquisition to an ftp site.

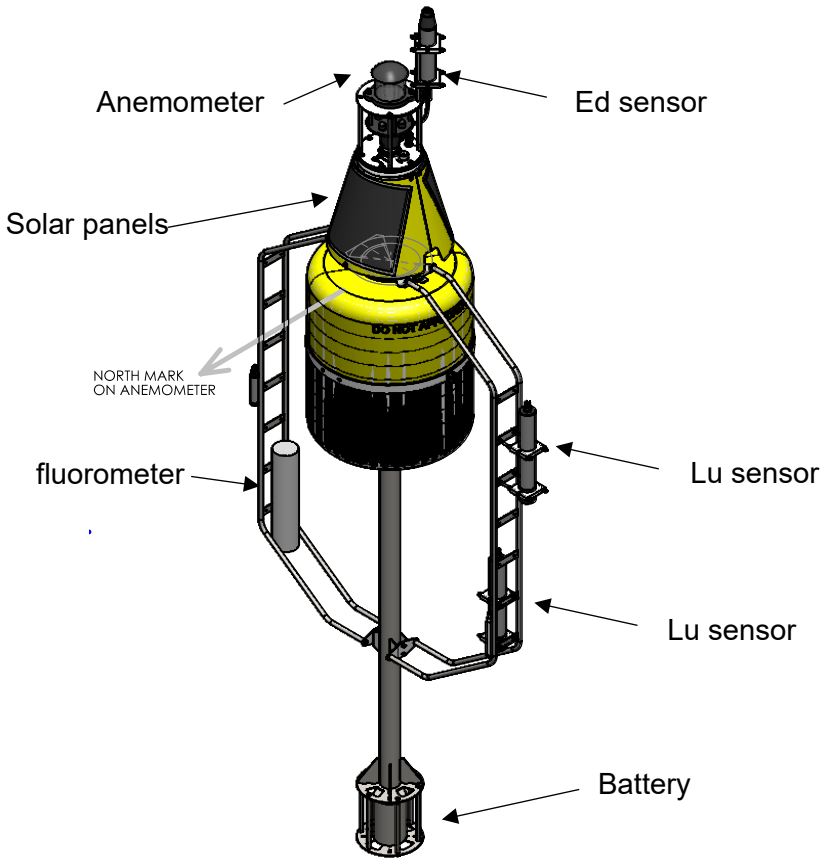

Figure 2: The autonomous radiometric Buoy displaying instrument payload. (credit: CSIR)

Processing of the autonomous radiometric data follows guidelines given by Mueller et al. (2003) and the processing scheme found in Antoine et al. (2008). Initial processing for remote sensing reflectance involves calculating a single median value for the burst acquisitions of $E_s(\lambda)$, $L_u(z_1, \lambda)$, and $L_u(z_2, \lambda)$. Using the two depth measurements of $L_u(\lambda)$, the upwelling nadir radiance just below the water surface ($L_u(0^-, \lambda)$) is calculated as follows:

$$L_u(0^-, \lambda) = L_u(z_1, \lambda) e^{K_L(z_1,\lambda) z_1} \quad (3)$$

Where z_1 is the radiometric sensor closest to the surface (z_1 = 0.15 m) and K_L is the diffuse attenuation coefficient for upwelling nadir radiance computed using the difference between the two sub-surface measurements of $L_u(\lambda)$:

$$K_L = \frac{\log[L_u(z_2,\lambda)/L_u(z_1,\lambda)]}{\Delta z} \quad (4)$$

A potential source of error when measuring the underwater light field is the instrument self-shading effect where the magnitude of the underwater radiance reaching the sensor detector is reduced due to self-shading by the sensor itself (Gordon and Ding, 1992). The error from self-shading was calculated according to equations in (Gordon and Ding, 1992). Using the corrected value for $L_u(0^-, \lambda)$, the water leaving radiance $L_w(\lambda)$, can be obtained as:

$$L_w(\lambda) = \frac{1-\rho}{n^2} L_u(0^-, \lambda) \quad (5)$$

where ρ is the Fresnel reflectance of the air sea interface, and n is the refractive index of water. The term $\frac{1-\rho}{n^2}$ is $\cong 0.55$ for freshwater systems (Palmer and Williams, 1974). Lastly, the remote sensing reflectance (R_{RS}) is calculated as the ratio of the water leaving radiance to total downwelling irradiance:

$$R_{RS} = \frac{L_w}{E_s} \quad (6)$$

2.4 Processing of OLCI data

After its launch in February 2016, OLCI went through a six-month commissioning phase in which radiometric data were only available to Sentinel-3 Validation teams (S3VT). Following a successful commissioning phase, as of October 2016 level-1 top of atmosphere products were made available to the public through the online Copernicus Open Access Hub of the European Space Agency (ESA). The level 1 data includes corrected, calibrated, spectrally characterized, and ortho-geolocated TOA radiance. Products can be acquired in Full Resolution (FR) 300 m pixel size or Reduced Resolution (RR) 1.2 km pixel size for full global coverage. The level 2 data products contain atmospherically corrected bottom of atmosphere (BOA) reflectance information along with geophysical products such as chlorophyll-a and total suspended solids calculated from standard level-2 operational algorithms. By the end of 2017, Sentinel-3A OLCI was fully operational with a full reprocessing of the sensors dataset from the commissioning phase onwards.

For S3VAL validation purposes, OLCI full resolution level-1 data were acquired using both he expert user's online data hub (which is only available to members of the Sentinel-3 Validation Team (S3VT) for validation purposes during the early stages of sensor operation) as well as the public open access hub. Image data were inspected and extracted using the open source Sentinel application platform software (SNAP). Processors for the SNAP software for further analysis were implemented using the snappy application programming interface (API) in

Python programming language. Subsets of the region of interest were extracted from the full image and corrected for small scale variations due to the non-central wavelength of a given band across the field of view, known as the smile effect.

In order to validate OLCI-based measurements of chlorophyll-a, TOA data and R_{RS} spectra were extracted from individual pixels based on GPS coordinates of in-situ data points. In-situ data was collected the same day as a Sentinel-3A overpass with a time difference of no more than four hours. Imagery was examined by-hand to determine valid match-up pixels that were also not contaminated by clouds or effects of high observational zenith angles (OZA) such as duplicate pixels. The models for deriving chl-a were then applied to the match-up dataset for the two full atmospheric corrections and three different stages of TOA data to retrieve chl-a estimates which were then compared to collected in-situ chl-a information and further error analysis.

2.5 Atmospheric modelling of in situ data to the top of atmosphere

MODTRAN radiative transfer software was used to propagate matchup R_{RS} measurements to TOA to assess radiometric sensitivity of OLCI for small inland water bodies. Using aerosol optical depth (AOD) and water vapour measured in-situ, the area-averaged (~2 km diameter) surface reflectance was retrieved from the OLCI image using MODTRAN. Area-averaged surface reflectance was used to calculate total atmospheric radiance at TOA for completely black pixel (black water, no water-surface reflectance). This MODTRAN run was also used to compute total downwelling irradiance at BOA. The total downwelling irradiance at BOA was used to compute the water-leaving radiance (L_w) at BOA via R_{RS} measurements performed in-situ around the time of overpasses.

The water-surface reflected sky radiance (using an upward-looking MODTRAN run in the correct viewing geometry) was added to L_w to obtain total upwelling radiance above water at BOA. Water-surface reflectance was interpolated from the Mobley (2015) look-up tables (assumed spectrally invariant for convenience). The total above-water upwelling radiance at BOA was multiplied by atmospheric path transmittance to obtain water-target radiance at TOA. The total atmospheric radiance was added to obtain the total water-target apparent radiance (sensor-observed) at TOA. All computations up to this point performed at full MODTRAN 5 spectral resolution. The OLCI spectral response functions were then applied to compute band radiances which were then compared to OLCI measurements at carefully selected pixels in the product. Corrections were applied to align the MODTRAN solar flux to the solar flux reported in the OLCI product.

2.6 Atmospheric corrections for OLCI

2.6.1 Case 2 Regional CoastColour

The original Case 2 Regional algorithm developed for the MERIS ground segment is a Neural Network-based approach where the atmospheric correction and derivation of inherent optical properties (IOPs) are coupled and solved for simultaneously (Doerffer & Schiller, 2007). The purpose of the NN is to derive water leaving radiance reflectance from radiance reflectance at top of atmosphere. The water leaving radiances are further defined by a database of inherent optical properties and concentrations based on a synthetic dataset of roughly 550,000 modelled reflectance spectra generated using HYDROLIGHT radiative transfer code. The inverse model derives three inherent optical properties from directional water leaving radiance reflectance for eight spectral bands of MERIS that are a product of the forward model, that which composes the atmospheric correction part of the algorithm. The procedure works as a coupled system where the water leaving reflectance and the inherent optical properties: total scattering of particles, phytoplankton pigment absorption, and absorption due to dissolved organic matter are derived simultaneously.

A major revision of the Case 2 Regional processor has taken place after subsequent modifications and testing and now incorporates the use with OLCI. The development was through the European Space Agency's CoastColour project whose mission is to expand MERIS and Sentinel capabilities to coastal and inland waters. The modified algorithm is termed the Case 2 Regional CoastColour (C2RCC) and incorporates the same foundation technology as C2R but has expanded to include a 5-component bio-optical model, a coastal aerosol model, and expanded bio-optical training ranges (Brockmann et al., 2015). The input to the C2RCC processor are OLCI level 1b top of atmosphere radiances. Outputs of the algorithm are the directional water leaving reflectance and the five IOPs. The absorption properties are split into total absorption along with a detritus component, a *gelbstoff* (dissolved organic matter) component, and the scattering properties are split into a white scatter and a sediment scatter. Analytical equations are then used to convert the IOPs to chlorophyll concentration.

2.6.2 6S Version 1

The Second simulation of a Satellite Signal in the Solar Spectrum (6S) is an advanced radiative transfer code based on successive orders of scattering (SOS) approximations designed to simulate reflection observed by a satellite sensor for a target at bottom of atmosphere using a coupled atmosphere-surface system (Vermote, 1997). The code has

been developed as a vector version known as 6SV which can handle radiation polarization (Kotchenova et al., 2006) and used operationally for the MODIS land surface reflectance product MOD09 (Vermote & Kotchenova, 2008) as well as the land surface product for Landsat 8/OLI (Vermote et al., 2016). The code has also been used quite extensively and successfully for atmospheric correction over water bodies for a variety of multispectral sensors (Matthews et al., 2010; Giardino et al., 2014; Martins et al., 2017).

The code was initially developed to propagate surface reflectance to satellite sensor altitudes, however, the code can be switched to atmospheric correction mode where the inputs are the sensor top of atmosphere radiances, sensor geometries, atmospheric and aerosol models, and ground target elevation which is assumed to be Lambertian. The outputs are bottom of atmosphere sensor radiances or reflectance. For the validation of OLCI products, the 6SV version 1.1 was applied using the Py6S Python programming language interface (Wilson, 2013). OLCI level 1b top of atmosphere radiances were collected for in-situ match-up points along with sensor geometries for each point.

Depending on the time of year of the fieldwork campaign, either a mid-latitude summer or mid-latitude winter atmospheric model was used. Aerosol information was obtained by a MicroTOPS II sunphotometer collected at time of overpass or from a nearby AERONET station located at CSIR Pretoria, South Africa. The code was run for each band of OLCI using defined spectral response functions with outputs in reflectance. Reflectance spectra were further divided by pi to obtain R_{RS} for comparison with the instrument and algorithm outputs.

2.6.3 Rayleigh scattering and absorption correction

Full atmospheric corrections over small eutrophic water bodies are generally laborious and often unsuccessful due to the complex nature of the optical signal and difficulty removing effects of interference from nearby land pixels known as the adjacency effect. When the target water body has a high particle load, as is the case for most South African inland water bodies, reflectance magnitudes are much higher than would be for clear water. This allows for spectral features to be identified at TOA, without having to introduce the uncertainty and error a full atmospheric correction would introduce.

The bottom-of-Rayleigh reflectance processor was applied to the validation data set as a simple atmospheric correction procedure to account for the effects of gaseous absorption in the red bands from water vapour, ozone, and molecular Rayleigh scattering (Matthews et al., 2012). The result is a TOA signal that has been normalized for gaseous and Rayleigh effects

and removes significant atmospheric absorption effects in the red and near-infrared (NIR) region of the spectrum where important spectral information pertaining to pigments can be identified. The Rayleigh correction in SNAP software was used to calculate Rayleigh corrected reflectance.

3 RESULTS AND DISCUSSION

3.1 Biogeophysical characteristics of study sites

The dams studied in the Gauteng Province are all quite similar in respect to the composition of their optically active constituents with phytoplankton and suspended sediments providing the bulk of the optical signal, thus classifying these dams as “bright” case-2 waters (Figure 3). Throughout all of the field sampling campaigns, high concentrations of algae and cyanobacteria persisted giving the water a green to brown coloration and noxious odour during times of scum conditions. Floating *Microcystis sp.* cyanobacteria colonies were clearly visible in the water. On certain occasions the concentration of floating colonies increased to create floating scum conditions. The Vaal Dam also consistently had high values of suspended sediment due to the high concentrations of illite clay suspended particles that reside in the dam. Table 5 shows statistics for the biogeophysical variables measured for surface and depth samples for all four dams.

Table 5: Biogeophysical variables from the three fieldwork campaigns

Dam	N	Min	Max	Mean	Median	St. Dev.
Roodeplaat						
Secchi (cm)	19	50	160	89.8	87.5	35.3
Chl (ug/L)	29	8.54	449	131.9	118.0	114.8
TSS (mg/L)	29	3.2	58.5	19.9	20.0	14.3
Hartbeespoort						
Secchi (cm)	8	50	315	205.5	209.5	75.5
Chl (ug/L)	8	4.5	215.3	70.1	33.5	90.7
TSS (mg/L)	8	0.8	28	7.2	4.8	9.0
Bronkhorstspruit						
Secchi (cm)	8	90	213	126.3	100.0	45.0
Chl (ug/L)	8	23.3	72.08	41.0	33.9	19.0
TSS (mg/L)	8	5	13	9.5	9.8	2.7
Vaal						
Secchi (cm)	4	10	20	17.5	20.0	5.0
Chl (ug/L)	4	47.03	520.2	231.9	180.1	218.0
TSS (mg/L)	4	8	84	37.9	29.8	33.3

Overall mean concentration of chl-a resulted in all four dams being classified as hypertrophic, however concentrations as low as 5 mg/l were measured at Hartbeespoort due to reduced nutrients from an infestation of water hyacinth. Water clarity was lowest in the Vaal dam owning to high concentrations of illite clay suspended in the water.

Figure 3: Images from fieldwork undertaken between June 2016 and November 2017.

Cyanobacterial species were the dominant microorganisms according to cell abundance across all dams and all depths with *Microcystis sp.* being the overwhelming majority (Table 6). Roodeplaat Dam regularly observed the highest cell abundances while the other three dams were considerably lower. The exception of this case was for Vaal Dam which was experience a wide-spread cyanobacterial bloom including surface scum conditions at the time of sampling.

Hartbeespoort dam has recently been experience massive hyacinth blooms in which the floating aquatic macrophyte has covered up to half of the dam. The dam generally experiences eutrophic to hypertrophic conditions mostly composed of cyanobacteria. However, the large amounts of hyacinth in the dam are taking up much of the nutrients in the water, leaving little

available for phytoplankton. The reduction in nutrient results in regions of the dam that are not covered by hyacinth to be more oligotrophic to mesotrophic with low chl-a concentrations.

Table 6: Statistics for phytoplankton by groups for each of the dams sampled.

Dam	N	Min	Max	Mean	Median	St. Dev
Roodeplaat						
Microcystis sp.	20	40182	557480	224275.4	203625	149359.665
BACILLARIOPHYCEAE	20	0	3258	809	181	990
CHLOROPHYCEAE	20	0	32942	9699	3258	11134
CRYPTOPHYCEAE	20	0	2534	559	362	657
CYANOPHYCEAE	20	40182	557480	227553	203625	151251
EUGLENOPHYCEAE	20	0	724	163	0	248
Total	20	40182	576666	238800.3	228241	154328.8656
Hartbeespoort						
Microcystis sp.	8	483	380617	62691	13300	130146
BACILLARIOPHYCEAE	8	186	4525	1628	1233	1316
CHLOROPHYCEAE	8	0	18703	7442	4861	8085
CRYPTOPHYCEAE	8	0	1809	728	647	651
CYANOPHYCEAE	8	483	451638	71812	13903	154871
EUGLENOPHYCEAE	8	0	362	88	0	164
Total	8	2655	462327	81700	32792	155457
Bronkhorstspruit						
Microcystis sp.	8	18100	400372	108753	52817	135111
BACILLARIOPHYCEAE	8	1086	2172	1534	1611	414
CHLOROPHYCEAE	8	0	9309	3759	3017	3146
CRYPTOPHYCEAE	8	0	690	300	362	268
CYANOPHYCEAE	8	19065	406164	114233	60747	133620
EUGLENOPHYCEAE	8	0	362	45	0	128
Total	8	23411	409784	119915	691325	132270
Vaal						
Microcystis sp.	4	63712	5792003	1780317	632777	2708258
BACILLARIOPHYCEAE	4	724	12670	5340	3982	5524
CHLOROPHYCEAE	4	0	724	181	0	362
CRYPTOPHYCEAE	4	0	1810	634	362	855
CYANOPHYCEAE	4	67332	5792003	1782127	634587	2706801
EUGLENOPHYCEAE	4	0	724	181	0	362
Total	4	68780	5806483	1788462	639293	2711994

3.2 Assessment of Sentine-3 OLCI

3.2.1 First look during commissioning phase

During the instrument commissioning phase, field measurements were made on 5 and 6 June simultaneous to OLCI overpasses (Figure 4). The automated Buoy was also deployed in Roodeplaat Dam at this time. Conditions on both days were cloud-free during the overpass time and collection of coincident in situ data. The image on 5 June had an observation zenith angle (OZA) of 14 degrees, whereas that on 6 June was 50 degrees. This accounts for the large increase in duplicated pixels on 6 June which is present at the edge of the image swath. There was a noticeable spatial offset in the images, due to a pointing error with the sensor. This resulted in a misalignment between the shapefile and the image. The spatial offset appeared to be larger on 6 June, likely related to the OZA.

The duplicated pixels are a result of the higher OZA towards the edge of the image swath (). Pixels at the edge of swath have a larger GSD which when resampled down to a 300 m resolution standard grid result in duplicate lines of pixels. Thus, the pixels are downscaled to a 300 m resolution, but are actually sampling an area larger than 300 m. This reduces data quality for small targets like Roodeplaat.

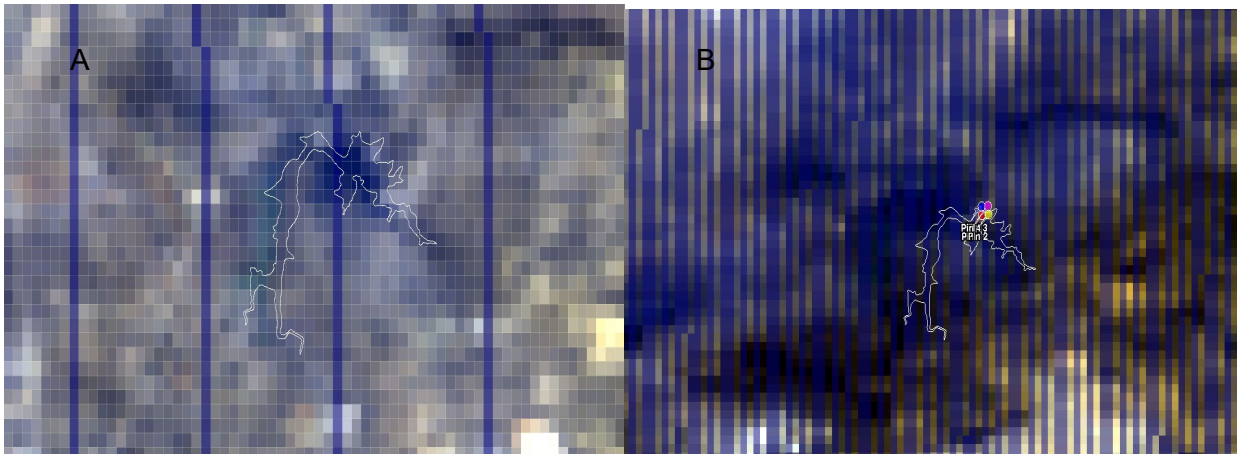

Figure 4: OLCI RGB image over Roodeplaat dam on A) 5 June 2016 and B) 6 June 2016. Duplicate pixels are indicated by dark blue whilst the shapefile for Roodeplaat dam is overlaid in white.

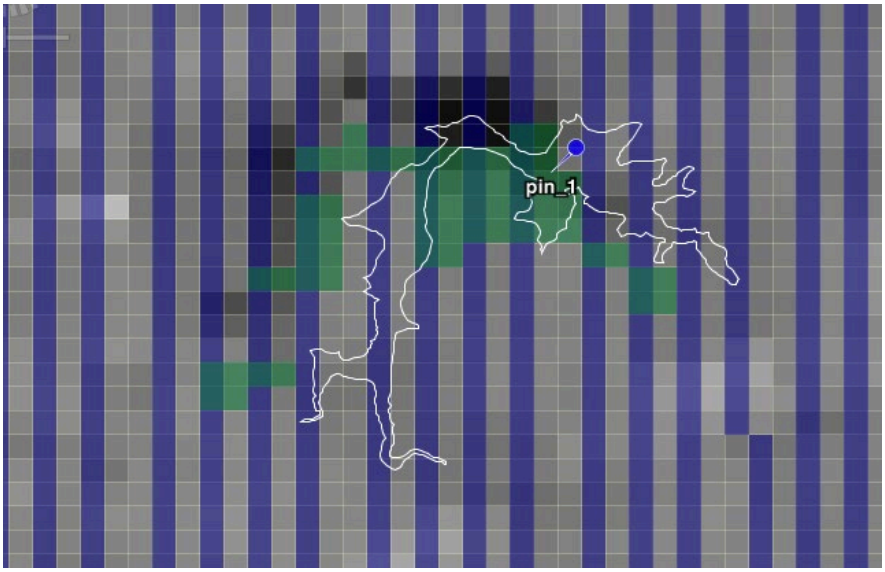

Figure 5: OLCI L1b band 17 TOA radiance measured on 25th June 2016 showing the spatial offset from the dark water pixels, the green fresh inland water body mask, and the white geo-located shapefile of Roodeplaat Dam and blue duplicate pixel lines. The pin marker represents the location of the Buoy.

A first look at the L1 TOA radiances extracted over Roodeplaat for the matchup dates are shown in Figure 6. The spectral shapes appear to be normal with good performance in all channels. The initial assessment of OLCI L1b TOA radiometry was as expected, depicting varying degrees of magnitude and spectral shape. The sensor appeared to be operating nominally.

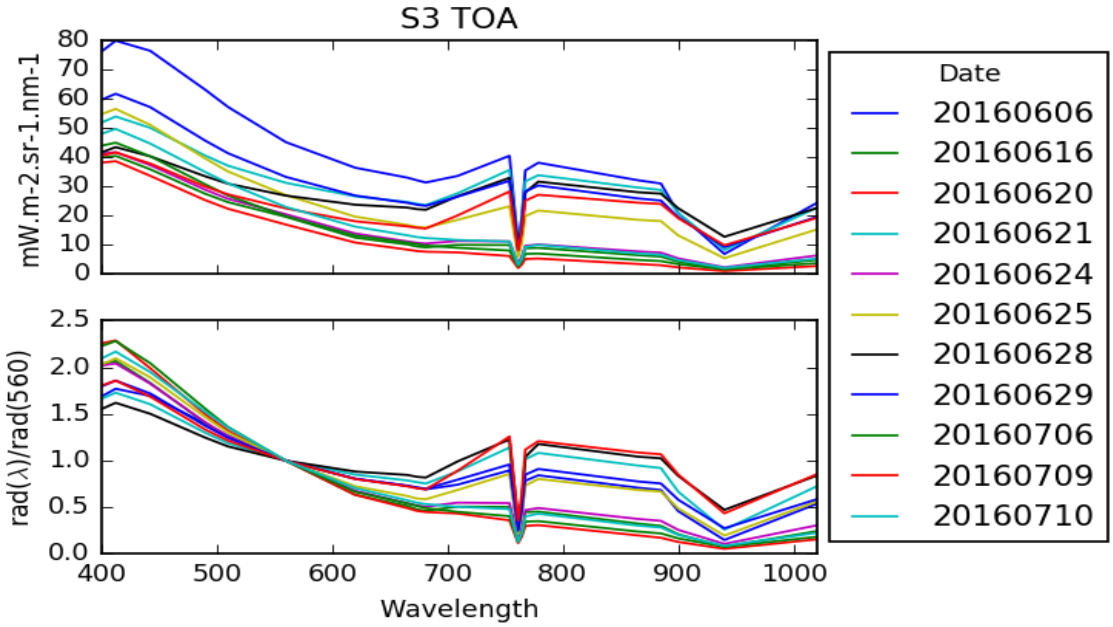

Figure 6: OLCI level 1b TOA radiance data (top) and radiance normalized to the 560 nm band (bottom) taken from Roodeplaat Dam.

The Case 2 Regional Coast Colour processor (C2RCC) was applied to OLCI L1 images of Roodeplaat Dam, where the Buoy was stationed (Figure 7, Figure 8, Figure 9). The algorithm was designed with turbid, case 2 waters and inland water bodies in mind, however, major disagreements are apparent. One issue is the large spatial offset induced by high OZAs: if the target is at the edge of swath, the resampled pixels create large numbers of duplicated pixels and spatial offsets that result in unusable imagery. It is evident that as OZA increases the number of duplicated pixels substantially increases. It is also important to note the spatial offset between the geo-coordinated shapefile and Buoy pin, the green fresh inland water mask, and the dark pixels representing the water body itself.

The C2RCC uses the pixels flagged as fresh inland water in its processing, while masking out the actual dark pixels as land. This is an important issue pertaining to atmospheric correction procedures over inland water bodies and requires further evaluation. The chlorophyll concentrations shown in the figures derived from the C2RCC processor also depict very low concentrations, much lower than what is typical for the dam. It must also be noted that no adjacency correction was applied so values may be significantly altered due to adjacency issues. From the C2RCC results, there was a decrease in chlorophyll concentrations with increasing OZA. Evaluation of Buoy measurements does not show a similar trend in chlorophyll concentrations for these dates (data not shown). This can have very concerning effects on derived products from Sentinel-3 and again, further evaluation is needed.

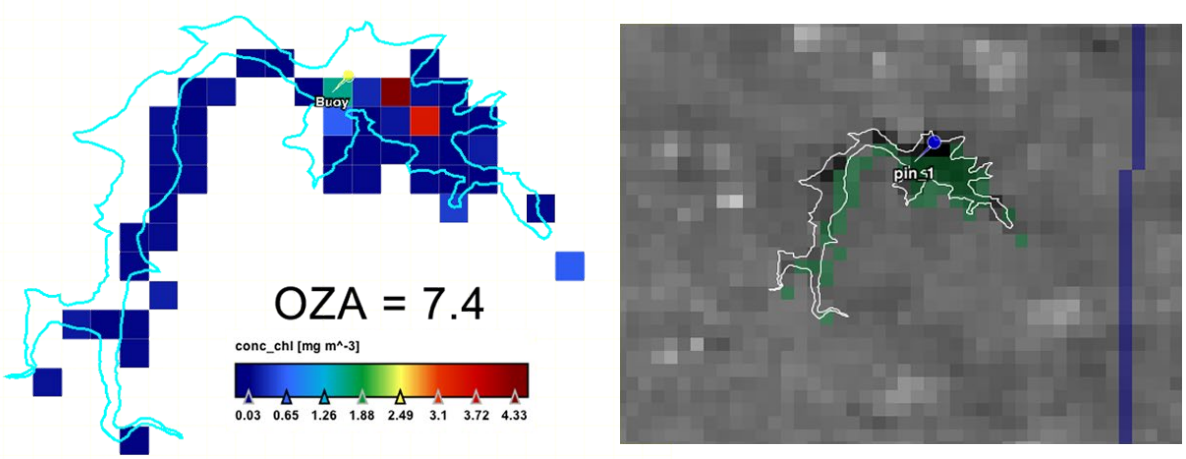

Figure 7: Chlorophyll concentration from Roodeplaat Dam from the Case 2 Regional Coast Colour Processor for the OLCI image on June 20th, 2016 and associated L1b image showing spatial offset and duplicated pixels.

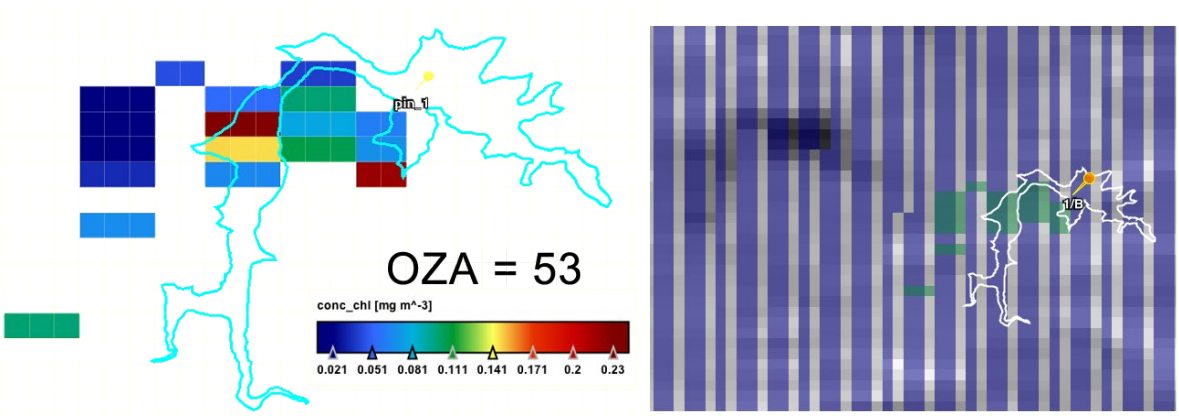

Figure 8: Chlorophyll concentration from Roodeplaat Dam from the Case 2 Regional Coast Colour Processor for the OLCI image on June 10th, 2016 and associated L1b image showing spatial offset and duplicated pixels.

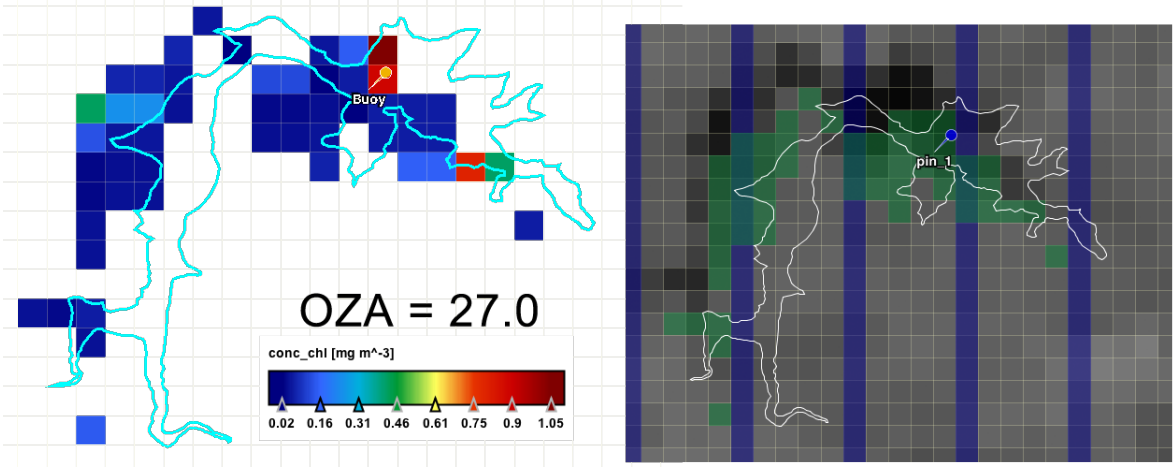

Figure 9: Chlorophyll concentration from Roodeplaat Dam from the Case 2 Regional Coast Colour Processor for the OLCI image of on July 10th, 2016 and associated L1b image showing spatial offset and duplicated pixels.

3.2.2 Assessment during operational phase

OLCI data was acquired for matchup dates during the fieldwork campaign between Oct. 25 and Nov. 3, 2016 (Figure 10). October 29 and November 2 were too cloudy to retrieve valid match up data with November 3 providing a partial image. Due to cloudy conditions, in-situ R_{RS} measurements from the ASD field spectroradiometer were only obtained at Roodeplaat Dam on Oct. 25 and Oct. 30. Improved geo-location was implemented in OLCI processing at the end of October which reduced the spatial offset that was observed during the commissioning phase in OLCI imagery at higher observation zenith angles (OZA).

The fresh inland water mask now correctly identifies inland water bodies, however, there is still a slight geo-location offset by a few pixels at higher OZA as seen by the shapefiles in Figure 10. Duplicate pixels as a result of higher OZA towards the edge of the swath remain an issue for small targets such as Roodeplaat Dam.

By examining a swath, the magnitude of the duplicate pixel effect is apparent (Figure 11). Toward the edge of the image swath the observation angle increases, which results in a larger ground sampling distance (up to 600 m at edge of swath). During image processing in the ground segment, the whole image is resampled to a 300 m resolution resulting in lines of duplicate pixels. Non-regular pattering in the distribution of duplicate pixels can result from the earth not being flat and from changes in altitude. The pattern of pixels is also caused by an aliasing effect since the resolution of the screen is not sufficient to display the nearly 4800 pixels across the track (pers. comm., Marc Bouvet).

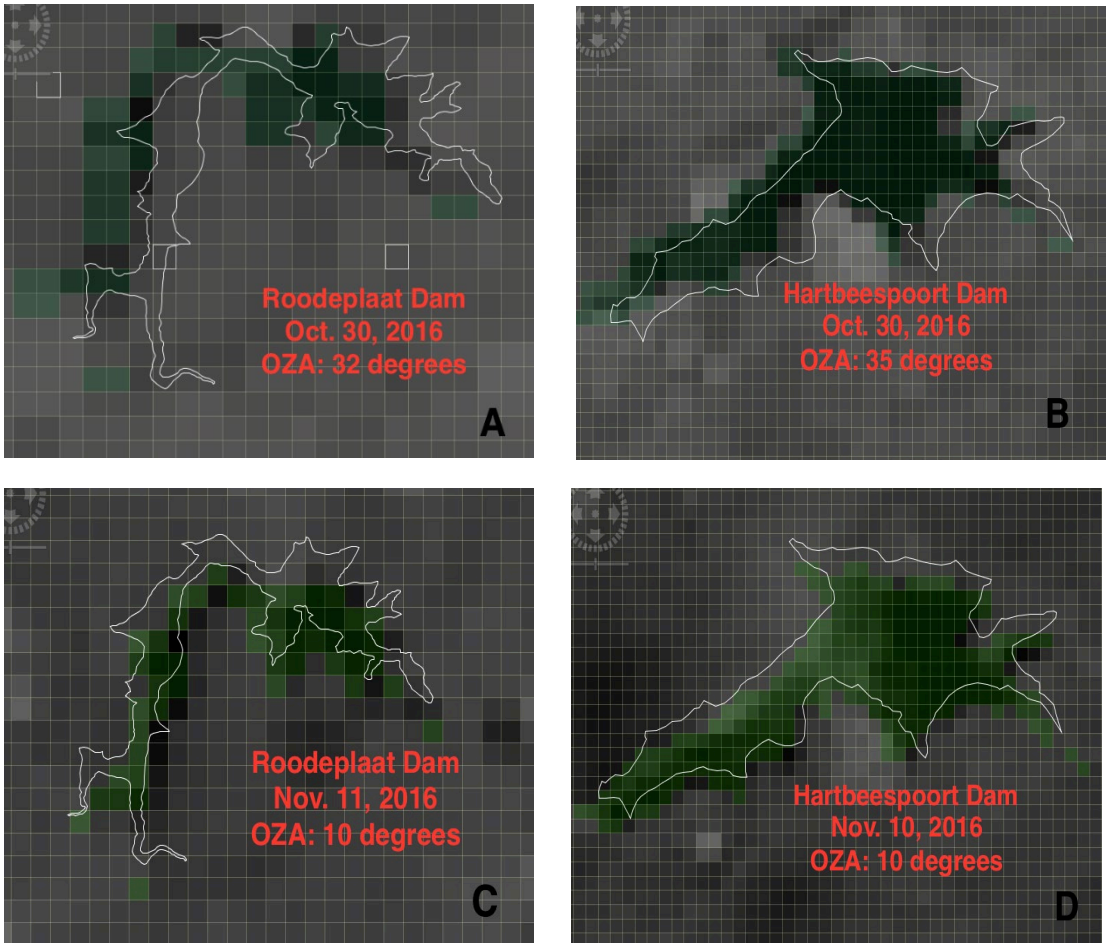

Figure 10: Roodeplaat and Hartbeespoort Dams as seen by OLCI (band 17 radiances). Water pixels can be clearly identified as darker pixels. The SNAP fresh inland water mask (green) and shapefile (white) show the improved geo-location.

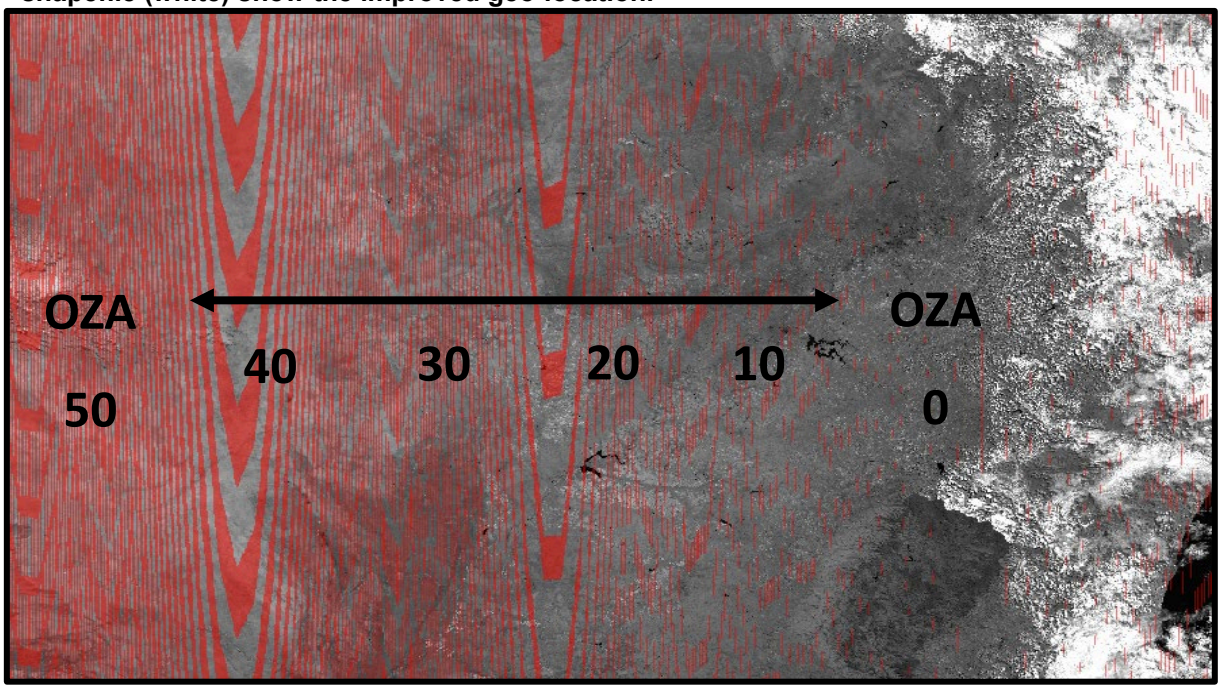

Figure 11: OLCI L1B Band 16 image over South Africa illustrating the increase in duplicate pixels with increasing OZA across the swath. Aliasing causes the illusion of patterns (see text).

3.3 Time series of measurements from an autonomous Buoy

The CSIR Buoy houses two subsurface triOS radiometers measuring upwelling radiance (L_u) at 0.15 and 0.76 m, and an above-surface radiometer measuring downwelling irradiance (E_d). Diffuse upwelling attenuation coefficients (K_u) are derived from the measured upwelling radiances, which is further used to propagate upwelling radiance from the shallower sensor to the surface (Figure 12). Remote sensing reflectance (R_{RS}) is calculated by propagating upwelling radiance through the air/sea interface and subsequently dividing by total irradiance. Buoy derived measurements look very comparable to measurements made in waters dominated by high biomass and presence of cyanobacteria.

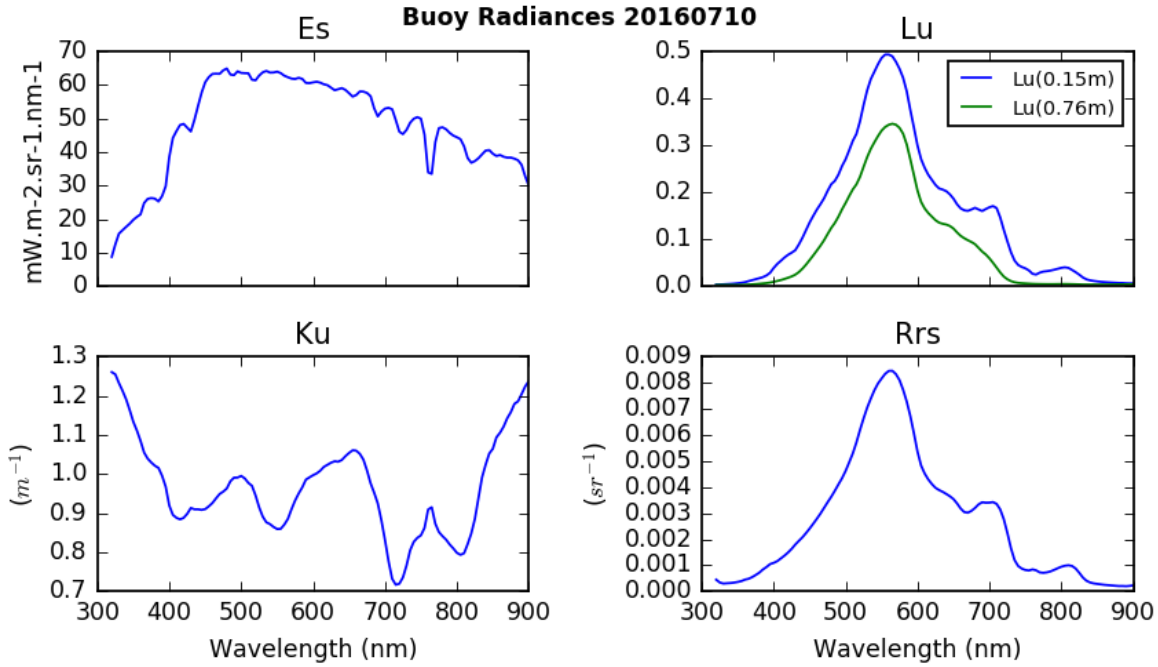

Figure 12: Downwelling irradiance, upwelling radiance at 0.15 and 0.76 m depth measured by the automated Buoy, and the calculated attenuation coefficient (K_u) and Remote Sensing Reflectance (R_{RS}).

Figure 13 shows a collection of remote sensing reflectance from various dates between 9th June and 17th July 2016. Colours correspond to associated concentrations of the cyanobacterial pigment phycocyanin and corresponding chl-*a* concentrations, calculated using simple reflectance relationships based on semi-empirical algorithms from Gons et al. (1999) and Simis et al. (2005, 2007). The algorithms were modified to incorporate use with the triOS sensor wavelengths. These algorithms were designed for use in turbid waters, and although no in situ water measurements were analysed for validation, the results give a good indication of pigment induced effects on spectral magnitude and shape of the reflectance. The results fall within reasonable ranges for the area and demonstrate the applicability for using

the Buoy as a validation tool. Figure 14 shows all R_{RS} measurements made from the Buoy at Roodeplaat Dam from 9th June to 5th August 2016.

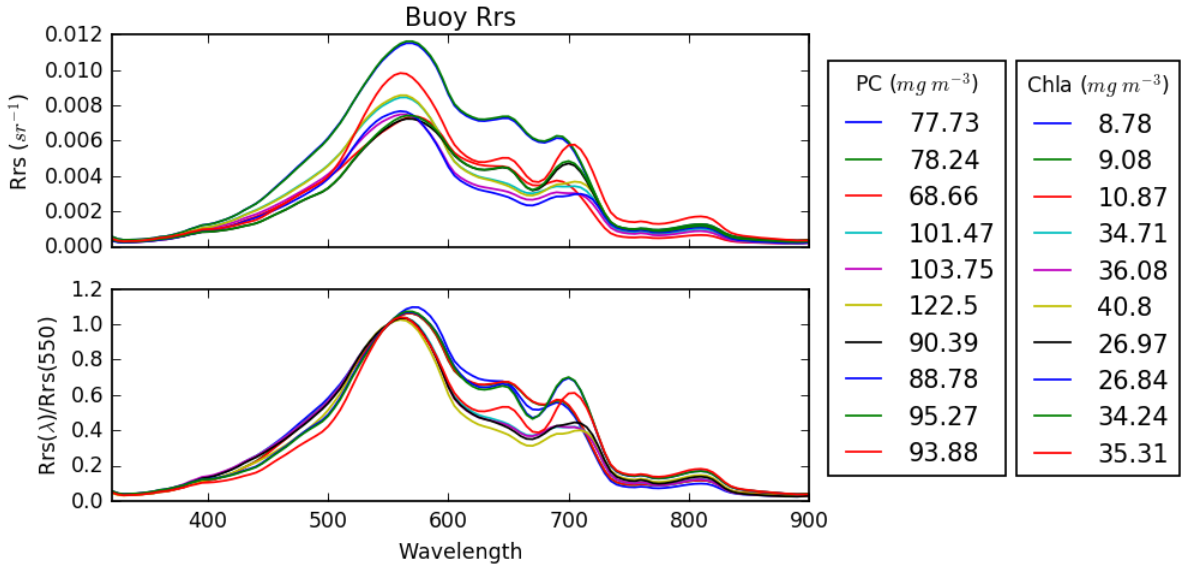

Figure 13: R_{RS} derived from the Trios sensors on the Buoy for specific dates in June and July 2016 and normalized to 550 nm (bottom). Colours indicate the estimated concentration of PC and Chl-a pigments.

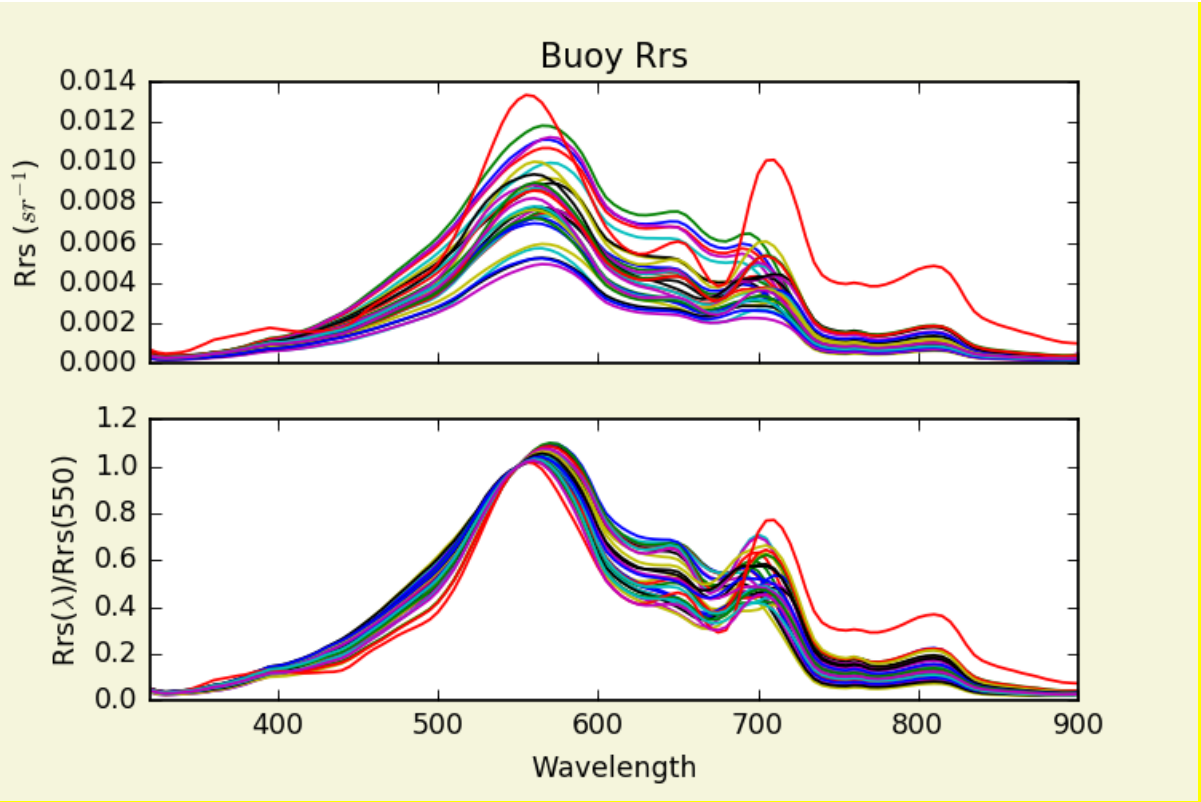

Figure 14: R^{RS} derived from the Trios sensors on the Buoy between June and August 2016 (top) and normalized to 550 nm (bottom).

Three different models for calculating chl-a concentration from R_{RS} measurements were tested using data from the Buoy: The 2-band empirical model (Moses et al., 2009), 3-band empirical model (Dall'Olmo and Gitelson, 2005), a band difference algorithm, the Normalized Difference Chlorophyll Index (Mishra and Mishra, 2012), and the previously described Gons and Simis semi-empirical algorithms. These were used to assess temporal changes in chl-a concentration during the time the Buoy was in Roodeplaat Dam.

Table 7: Comparison between chl-a measured in the laboratory and that estimated using the Gons, 2-band, 3-band and NDCI models.

Model	G08	2 Band	3 Band	NDCI	in-situ
Chl-a (μg/l)	38.6	44.1	41.5	30.7	43.03

These models exploit the red chlorophyll-a absorption peak around 675 nm to quantify chl-a concentration and have been used quite successfully to estimate chl-a concentrations in turbid, productive waters using in-situ radiometric data, or atmospherically corrected R_{RS} data from MERIS/MODIS (Gaunter et al., 2010; Gons et al., 2005; Moses et al., 2009; Gurlin et al., 2011). Bands used in the models were modified to incorporate use with the triOS sensor wavelengths. Model coefficients were taken from the literature references. Both the 2-band and 3-band coefficients were taken from Moses et al., 2009. This was done to assess the potential for using radiometry from an autonomous Buoy to derive a time series of pigment concentrations; however, only one simultaneous laboratory measurement of chl-a was made simultaneous to the Buoy measurements for validation. Although the models were not calibrated to South African water bodies, the estimated values compared closely to chl-a measured in the laboratory on 20th June 2016 (Table 7). The in-situ sample point was also taken a few hundred meters away from the Buoy itself but the concentrations derived from the 2-band (b2Chl), 3-band (b3Chl), and Gons (G08) models are very close to that measured in the lab; the NDCI (ndciChl) model underestimated chl-a.

The time series showed that each of the models followed similar trends throughout the duration the Buoy was deployed at Roodeplaat Dam (Figure 15). The time series uses data collected at 10 AM on each day between June and August 2016. Gaps result from cloud cover during which radiometric measurements are unusable. Chl-a concentrations varied from a minimum of 5 μg/l to a maximum of 120 μg/l, with an average around 50 μg/l. The significant difference between the models and the measured chl-a fluorescence is caused by dominant cyanobacteria sp. Cyanobacteria possess reduced chl-a fluorescence, due to the

arrangement of their pigments in the cells. This causes a lack of fluorescence signal and occasional miscorrelation with lab chl-a measurements.

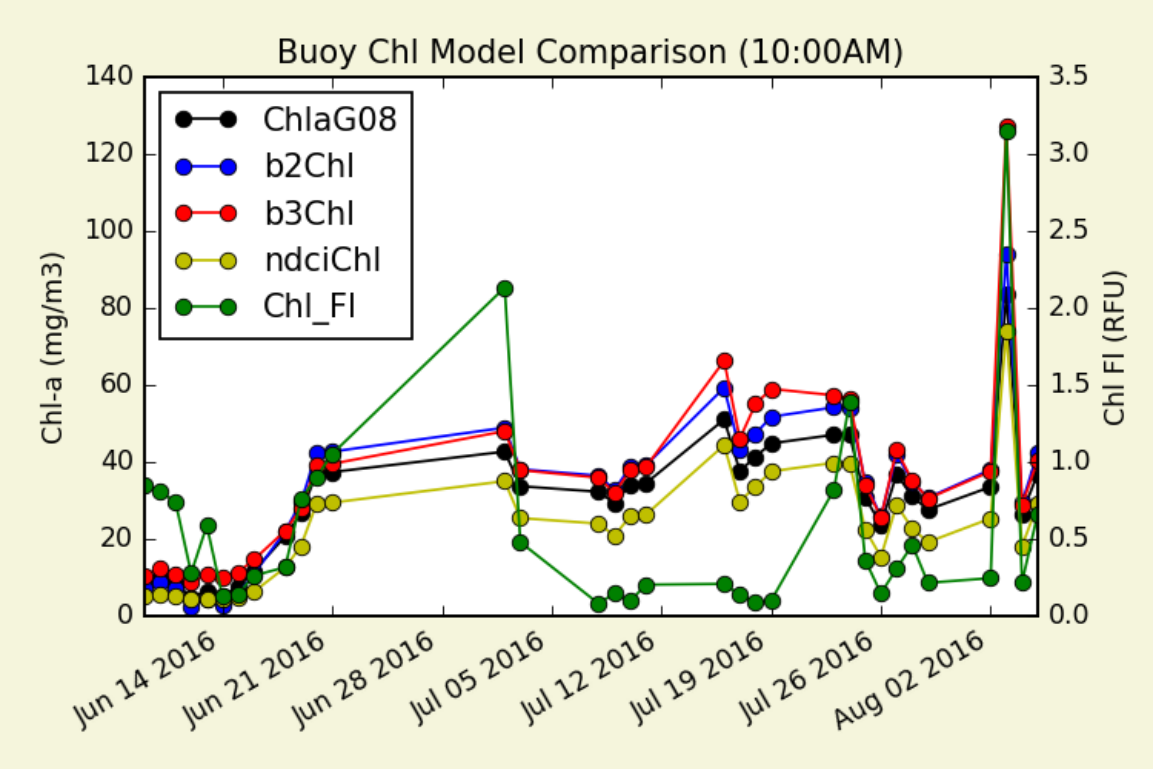

Figure 15: Chl-a concentrations estimated from the four models from June 9 to August 5, 2016 derived from Buoy R_{RS}. The green line is Chl-a fluorescence from the Buoy fluorometer

The Gons and Simis models were also used to assess temporal trends of PC and associated backscattering. PC is the dominant pigment associated with cyanobacteria and can act as an indicator of cyanobacteria biomass (Simis et al., 2005; 2007). Figure 16 and Figure 17 show the three month and daily variability, respectively. The abundance of cyanobacteria in the water is indicated by elevated PC concentrations, which are higher than those for chl-a. Cyanobacteria typically contain more PC than chl-a, as it is their primary light-harvesting pigment. Cyanobacteria contain vacuoles which help to regulate their buoyancy in the water column, but can also increase spectral backscattering (Matthews et al., 2013).

Figure 17 shows that the daily variability in chl-a at a single point can range from 15 to 20 μg/l. This change can be quite significant when considering bloom periods and has implications for temporal and spatial resolutions required to monitor dynamic, eutrophic systems. It also highlights the necessity of having matchups within a few hours of satellite overpass times for precise algorithm validation. The large changes in fluorescence could be caused by vertical

movements of cyanobacteria in response to wind and mixing of algae and cyanobacteria over hourly time scales.

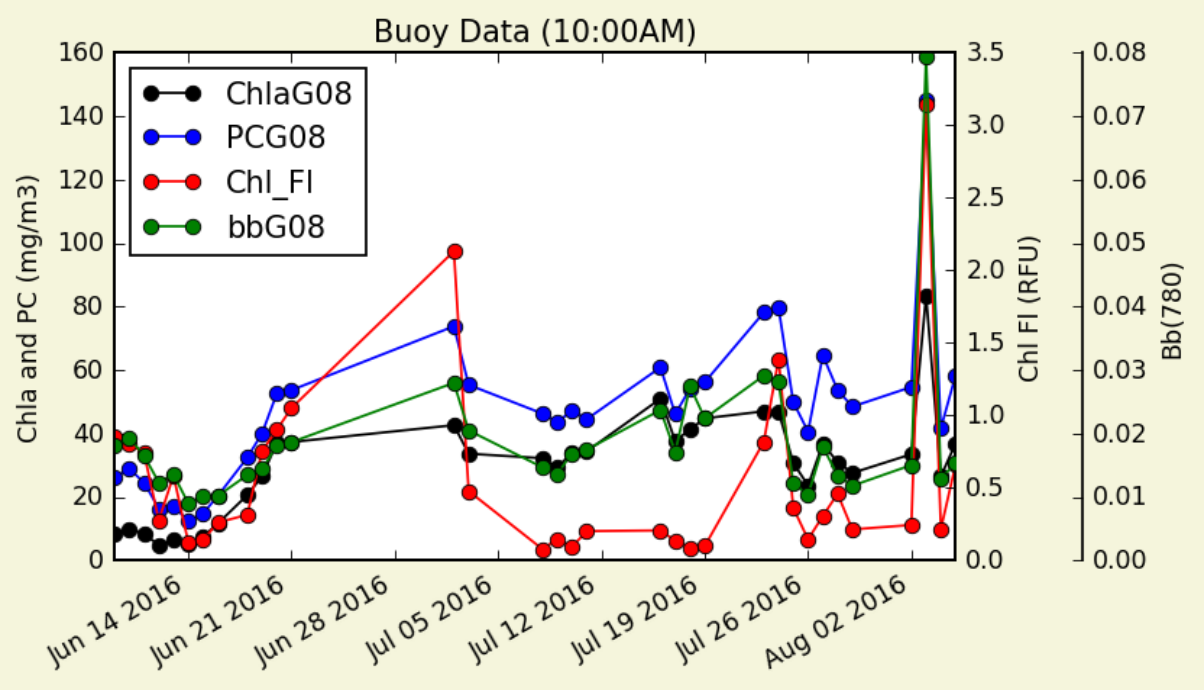

Figure 16: A three-month time series of chl-a, PC, backscattering (bb) and chl-a fluorescence measured between 9th June to 5th August 2016 (calculated from the Gons and Simis algorithms).

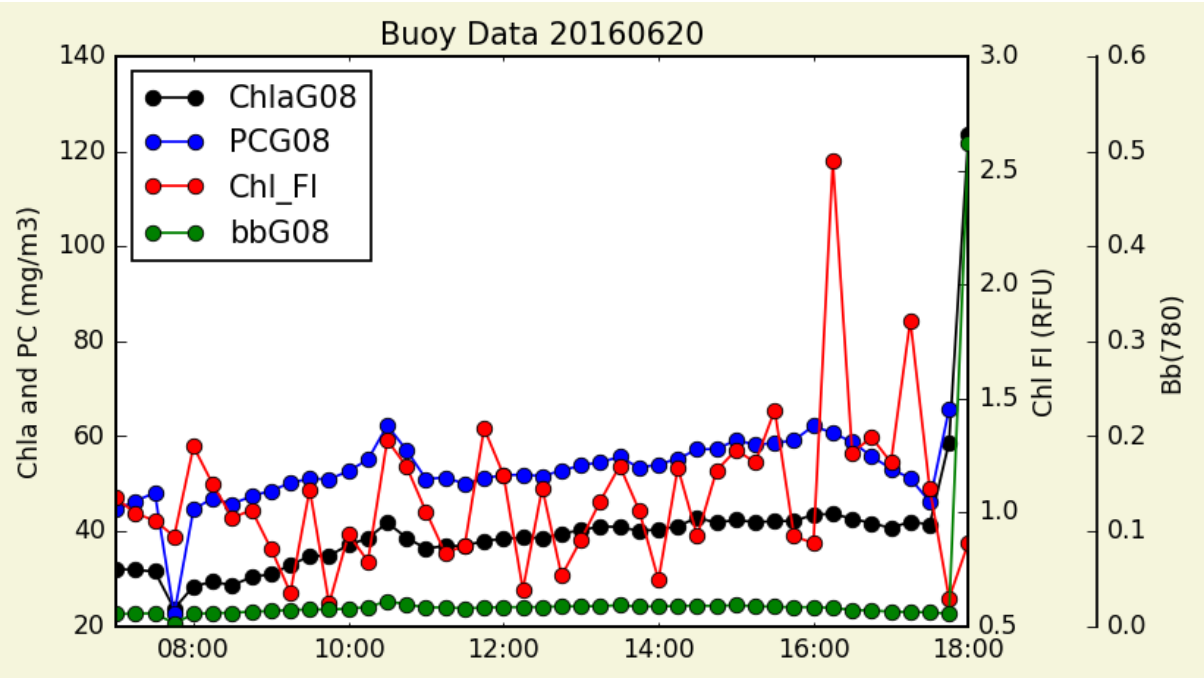

Figure 17: A daily time series from 20 June 2016 showing the daily variation in chl-a, PC, and backscattering (bb) and chl-a fluorescence (calculated from the Gons and Simis algorithms).

3.4 Water leaving reflectance characteristics

In situ measurements of reflectance were acquired during all four field campaigns in addition to that acquired by the Buoy. These data are essential for validating the spectral features observed from space by OLCI. The combined dataset of R_{RS} is plotted in Figure 18. There were large differences in magnitude and shape in reflectance spectra throughout the year. Data acquired during different field campaigns distinctly show different "water types" based mainly on the concentration of phytoplankton, and more specifically *Microcystis* cyanobacteria, in the water. The first measurements from June are from lower biomass waters ranging from roughly five to 30 ug/l chl-a. The Oct/Nov 2016 sampling campaign had chl-a values ranging from roughly 30 to 450 ug/l chl-a with much higher counts of *Microcystis sp.* As a result we see greater magnitude in reflectance and more clearly defined peaks at around 550, 660 and 710 nm. The March/April 2017 sampling had similar ranges of chl-a to October/November 2016, however skewed more towards higher concentrations when floating *Microcystis* colonies formed scum conditions. The final fieldwork campaign sampled during the spring of 2017 experienced relatively mild bloom conditions.

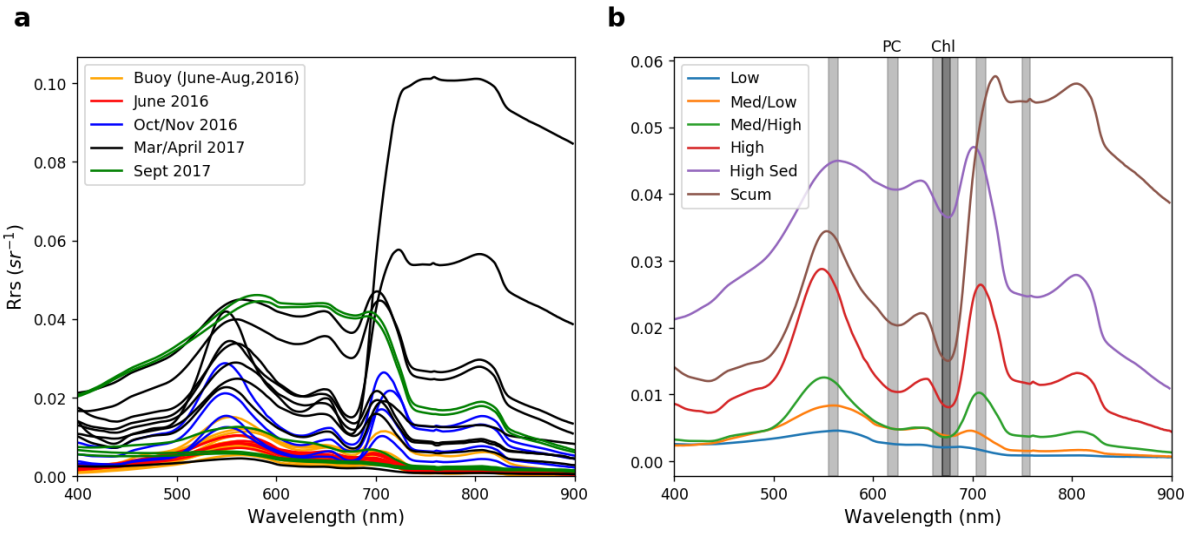

Figure 18: Remote sensing reflectance data collected during field work and by the automated Buoy (a), and examples showing various chl-a concentrations overlaid with the OLCI spectral bands (b).

The majority of the measurements were obtained at Roodeplaat Dam where *Microcystis* colonies were almost always present. Thus, reflectance exhibited a trough at 620 nm attributed to the strong absorption of the cyanobacterial pigment phycocyanin (PC). As concentrations of chl-a reach about 10 ug/l, the specific absorption of chl-a also begins to dominate the chl-a fluorescence peak around 675 nm and forms a trough (Bidigare et al., 1990). The magnitude of the trough at 675 nm varied by over two orders of magnitude ranging from 0.002 sr^{-1} to

0.041 sr^{-1}. The troughs at 620 and 680 nm produce a prominent peak in the 654 nm region, which is also aided by the PC fluorescence maximum at 650 nm. A very strong peak is also evident around 709 nm due to the phytoplankton absorption trough at 675 nm and the strong absorption due to water (Gitelson, 1992; Gons, 1999). Magnitudes of this reflectance peak varied by almost five orders of magnitude from 0.0016 sr^{-1} to 0.076 sr^{-1}. Strong backscattering at high concentrations causes the peak at 709 nm to also become more pronounced.

Bronkhorstspruit Dam experienced similar conditions as Roodeplaat but generally did not get to as high concentrations of chl-a and had much lower percentage of *Microcystis* in the water, leading to less pronounced PC related spectral features. Unfortunately, only one reliable reflectance measurement was able to be obtained at Hartbeespoort Dam, but this measurement resembled that more of oligotrophic, eukaryotic dominated water with elevated reflectance in the blue/green region and a small reflectance peak around 681 nm characteristic of chl-a fluorescence.

Hartbeespoort Dam has the potential to have large swings in trophic status as periodically the dam becomes covered in the aquatic macrophytes. These macrophytes, most commonly water hyacinth, take up the majority of the nutrients in the dam resulting in very low chl-a concentrations. During periods of when macrophytes are absent, Hartbeespoort typically displays hypertrophic conditions with cyanobacterial scums with reflectance signatures resembling those measured at Roodeplaat.

The Vaal dam experienced super-scum conditions which can be seen by the highly elevated signal in the red and NIR. Vaal Dam has high concentrations of clay illite (Birch, 2001) which results in reflectance typical of sediment dominated waters with a broad increase in reflectance magnitude between about 550 and 700 nm due to increased backscattering from the increased particle load. However, peaks around 660 and 710 nm are still prominent from high cyanobacteria abundance. The positioning of the OLCI bands exploit the effects related to PC and chl-a absorption features as seen in Figure 18.

The reflectance in the blue spectral region was highly restrained due to strong absorption by chl-a as well CDOM and tripton. The variable presence of these other constituents generally results in poor performance of blue/green-based chl-a algorithms (Gurlin et al., 2011; Gitelson et al., 2009). The peak at 550 nm varied by an order of magnitude ranging from 0.0044 sr^{-1} to 0.044 sr^{-1}. This is mainly due to the high variability of chl-a concentrations as this peak is typical of algal cells, mostly due to the low absorption of chl-a in the region. There is some reflection of sky light visible by enlarged reflectance at wavelengths less than 450 nm due to

the appearance of overhead clouds or haze and smog effects from biomass burning in the region (Doxaran et al., 2004). This effect sometimes led to unreliable radiance measurements which had to be discarded. Overall the reflectance features are typical of eutrophic waters with high concentrations of cyanobacteria and algae (e.g. Qi et al., 2014; Gitelson et al., 2008; Moses et al., 2009b).

3.5 Assessment of OLCI top of atmosphere radiances

Water leaving reflectance measured at the surface co-incident with OLCI overpasses were modelled to TOA in order to assess the relative performance of OLCI. This gives a rough indication that the radiances measured by OLCI are indeed indicative of those being measured on the ground, and that excess stray light entering the sensors field of view does not severely contaminate the data at TOA. A comparison between OLCI and the radiances computed by atmospheric modelling are presented in Figure 19.

Results for Hartbeespoort and Bronkhorstspruit dam are quite successful with the modelled radiance maintaining very similar shapes and magnitudes. The modelled radiances for Roodeplaat Dam maintain similar spectral shapes while the radiances were under-propagated throughout most of the vis-NIR spectrum with greater differences in the red/NIR and blue regions. This could be due to the mischaracterization of atmospheric parameters or due to not characterizing the signal due to the adjacency effect well enough. The chl-a concentrations were also much higher which complicates the signal.

The Vaal Dam experienced surface scum conditions with high sediment loads. Modelled Vaal radiances over-propagated in the NIR, but were under-propagated in the visible. This is most likely due to errors in propagating the cyanobacterial scum signal. These effects will require further investigation. The results do show, however, that OLCI sensitivity is high enough to still resolve required spectral features in a region with a complicated atmospheric signal and is evidence that OLCI sensor quality is high enough for inland water applications. A proper characterization of atmospheric parameters and contribution of adjacency signal would likely lead to improved modelling results.

Importantly, the results demonstrate that OLCI effectively characterized the signal at TOA evidence that it is a highly sensitive and well-calibrated radiometer suitable for sensing dark water targets. It also demonstrates extremely robust performance across all visible channels of the radiometer.

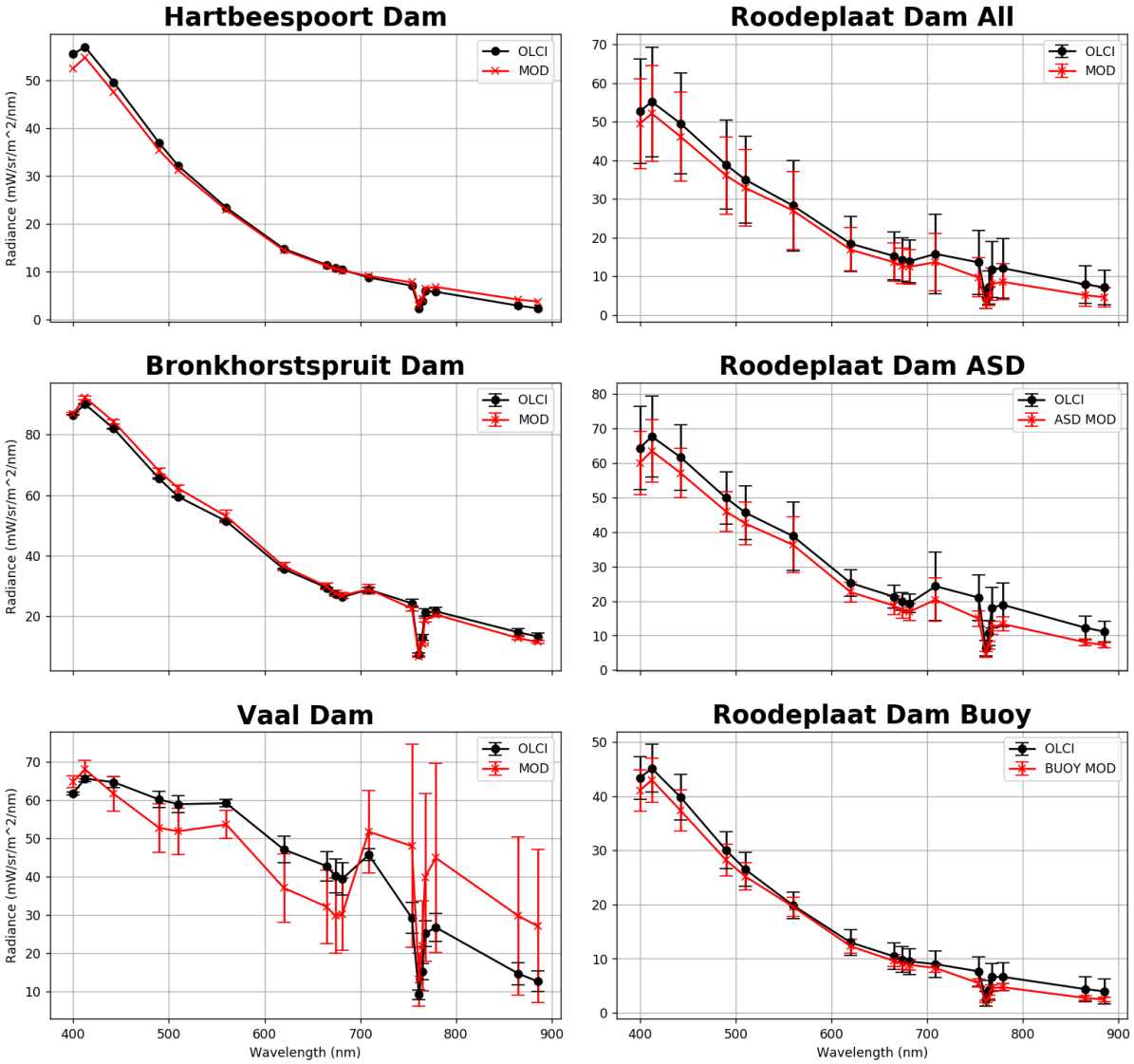

Figure 19: Comparison between radiances at TOA measured by OLCI and that modelled using MODTRAN from water leaving reflectance. Black lines are OLCI observed L1b radiances, red lines are modelled radiances. Error bars are the standard deviation of the mean.

3.6 Assessment of atmospheric corrections applied to OLCI

3.6.1 Performance of standard atmospheric corrections

The performance of two atmospheric corrections were assessed for deriving water leaving reflectance (R_{RS}) and compared to measurements made simultaneously at the water surface. The Case 2 Regional Coast Colour processor (C2RCC) was designed with turbid, case 2 and inland water bodies in mind, however, major disagreements were apparent between in situ measurements and that derived from OLCI (Figure 20). The dams in South Africa frequently experience concentrations of optically active constituents out of the training ranges for the neural net in C2RCC. It is also our assumption that the atmospheric properties in South Africa

are outside of the training ranges of the neural net and thus make a successful atmospheric correction very difficult. This is more than likely the major cause of the disagreement.

The region is dominated by high amounts of biomass burning particles as previously described. These small, high scattering particles are not well characterized in the neural network training datasets and thus the algorithm fails to properly parametrize the aerosol loading. Only one comparable result was obtained at Hartbeespoort dam when the chl-a concentration was below 10 mg/m^3. The rest of the corrections are all vastly overcorrected throughout the entire spectrum with little to none of the spectral features relating to chl-a or phycocyanin present. The Vaal dam data shows a rough peak in the green region and a small peak in the scattering region around 709 nm, however, magnitudes are much reduced.

This finding is significant and illustrates that out-of-the-box algorithms trained with marine-dominated datasets are unsuitable for use in small inland water bodies. This confirms earlier studies that have demonstrated the need for alternative types of atmospheric corrections, such as those that use spatial interpolation (see Guanter et al., 2009). Thus, the likelihood that C2RCC (and similar approaches) could serve as an accurate atmospheric correction in inland waters is very low or null.

The Second simulation of a Satellite Signal in the Solar Spectrum (6SV1) is an advanced radiative transfer code based on successive orders of scattering (SOS) approximations designed to simulate reflection observed by a satellite sensor for a target at bottom of atmosphere using a coupled atmosphere-surface system (Vermote, 1997). Unlike C2RCC which is a fully image-based atmospheric correction, 6SV requires the input of atmospheric parameters and sensor geometries. This often means that its use is not practical or feasible in operational application, thus it is not regularly implemented as a correction scheme. In order to provide input data, OLCI L1b TOA radiances were collected for in situ matchup points along with sensor geometries for each point, with atmospheric data retrieved from MicroTOPS or Aeronet measurements nearby.

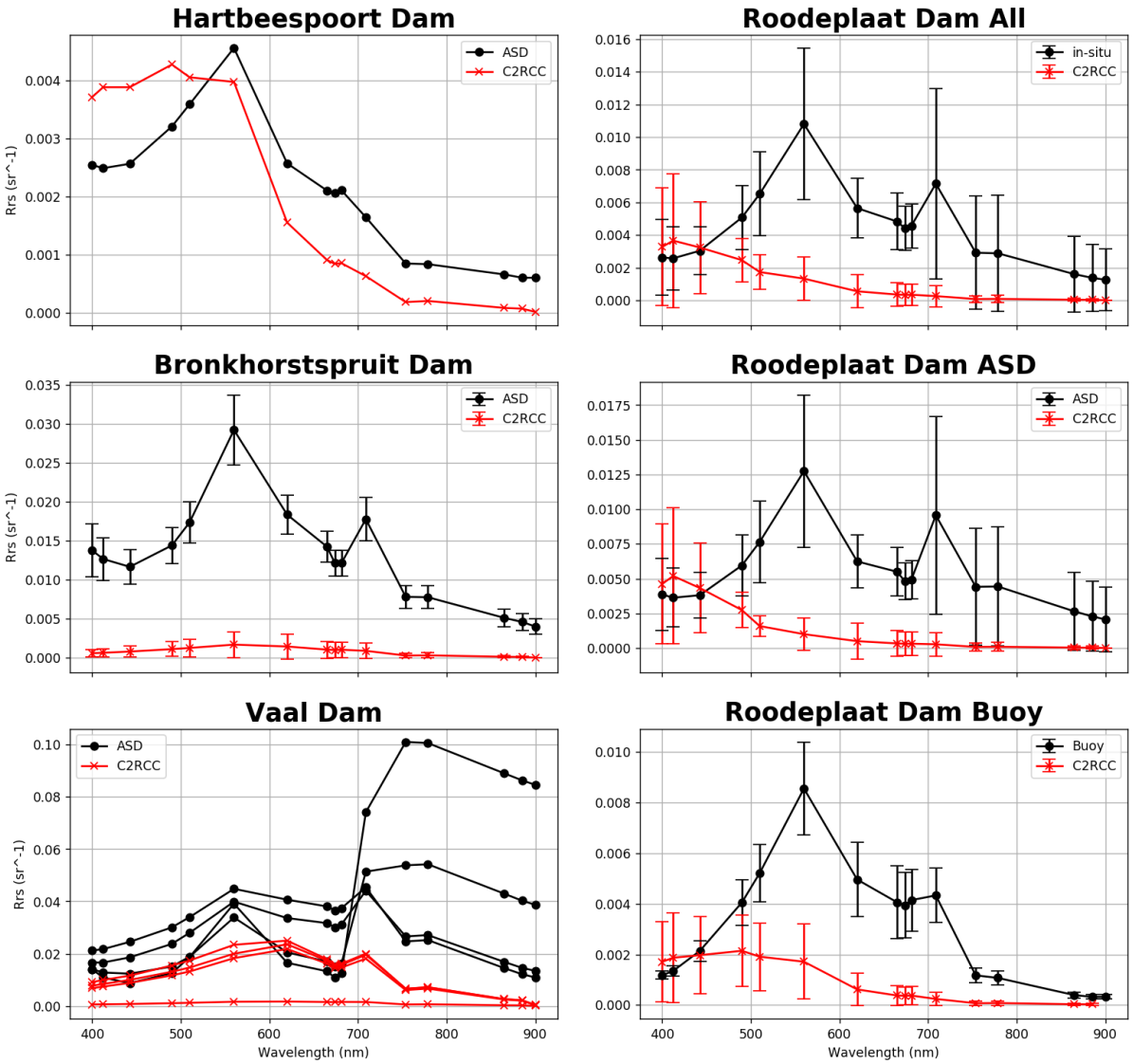

Figure 20: Atmospheric corrections using C2RCC for match-up dates. Black lines are ASD or Buoy derived R_{RS}, red lines are atmospherically corrected R_{RS}. Error bars are the standard deviation of the mean.

Results from 6SV1 are significantly improved compared to C2RCC; however apparent differences between the in situ and corrected reflectance exist, primarily in the red and NIR (Figure 21). Consistent under-correction of the reflectance in the red/NIR is likely due to unaccounted for stray light reaching the sensor from brighter land and vegetation surrounding the water pixels. This stray light (called the adjacency effect) bleeds into pixels and is particularly strong in the red and NIR. It is also apparent that the band at 400 nm, which is more strongly affected by aerosol particle scattering and absorption, is very poorly corrected. This is evidence of a complex atmospheric signal that is difficult to characterize due to the presence of many small particles.

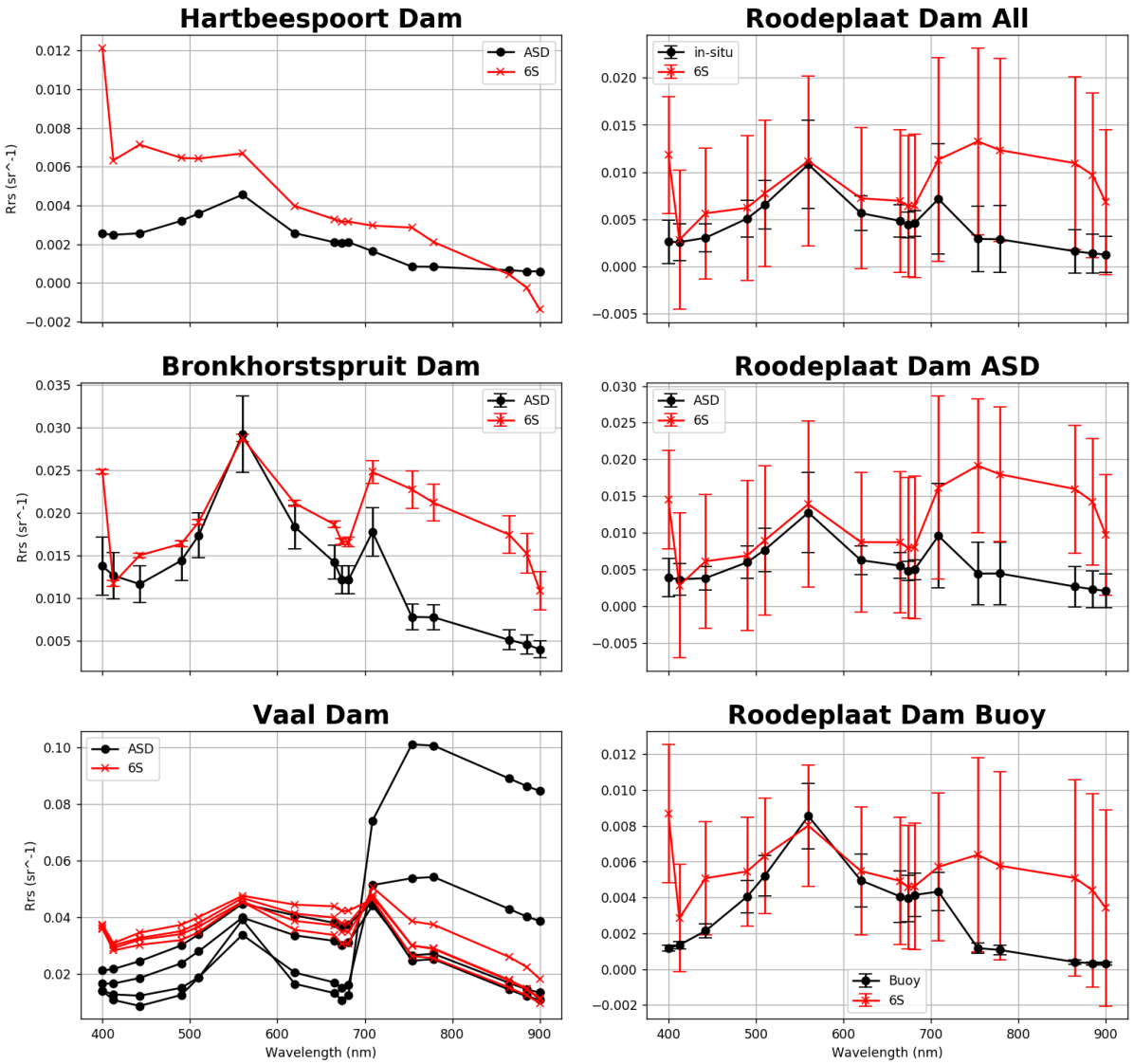

Figure 21: Atmospheric corrections using 6SV1 for match-up dates. Black lines are ASD or Buoy derived R_{RS}, red lines are atmospherically corrected R_{RS}. Error bars are the standard deviation of the mean.

The standard deviation of the corrected reflectance was also quite high, depicting variable performance in the correction. Unexpectedly, 6SV1 seems to have over-corrected the bright NIR reflectance characteristic of surface scum conditions at the Vaal. This is problematic because detection of bright blooms is an essential task of remote sensing from space. This highlights the importance of utilising an accurate and reliable atmospheric correction, and also the risks associated with utilising unsuitable or poorly characterised methods. The risks present themselves in misidentified blooms, or poor correlation between satellite and ground measurements caused primarily by inaccurate atmospheric correction. Despite the finding that OLCI is an extremely robust and accurate sensor (Section 0), the lack of a suitable atmospheric correction that is easy to implement hinders many applications for inland waters.

3.6.2 Variability of atmospheric aerosols

The degree to which variability in atmospheric aerosols causes the difficulties observed with atmospheric corrections is assessed here. Aerosols are attributed to the fine scale liquid and solid suspended particles in the atmosphere except for cloud particles and ice crystals and accounts for high absorption of radiative energy in the visible and NIR region. Aerosols and columnar water vapour are the most variable atmospheric constituents that can have large implications on water leaving radiance retrieval (Bassani et al., 2015). Aerosol optical thickness (AOT) gives information on the attenuation of light in the atmosphere related to the aerosol load in the vertical column of the atmosphere with higher AOT's representing higher attenuation and lower visibility (Wang and Christopher, 2003). Aerosol loading was measured at time of OLCI overpasses at wavelengths 440, 500, 550, 675, 870 and 936 nm using a microTOPS sunphotometer. AOT at 550 nm was derived after fitting the Angström power law to the measured AOT values and used to represent the total aerosol loading at that time of measurement.

The Cimel CE318 robotic sunphotometer located at CSIR Pretoria was also used to derive AOT at 550 nm and was compared to the microTOPS measurements (Figure 22 A). AOT at 550 nm showed high variability over the various sampling periods with values as low as 0.12 measured with the microTOPS and 0.07 measured at the Aeronet station at CSIR with maximums reaching 0.58 and 0.4, respectively. The microTOPS generally had a positive bias compared to Aeronet measurements. However, it must be noted that Roodeplaat, Hartbeespoort, Bronkhorstspruit, and the Vaal are roughly 15, 42, 43 and 130 km away from the Aeronet station, respectively. At very small spatial scales (< 30 km) it can be assumed that the aerosol properties are constant (Guanter et al., 2007).

Holben et al. (1991) also found that at a 90% confidence level, aerosol properties can only be extrapolated to a distance of about 20 km with an error of 50%. Thus, it is unlikely that the data from locations other than Roodeplaat are strictly comparable. However, Moore et al. (2013) found that AOT could be considered homogeneous for a radial distance of 100 to 150 km over southern India, as inferred from MODIS data. Thus, the variability of aerosol properties between Roodeplaat Dam and the Aeronet station can for the purposes of this study be considered comparable. The positive bias most likely comes from drifts in calibration of the microTOPS. The microTOPS channel at 440 nm was also unavailable, and therefore unable to be included in the calculation of AOT-550.

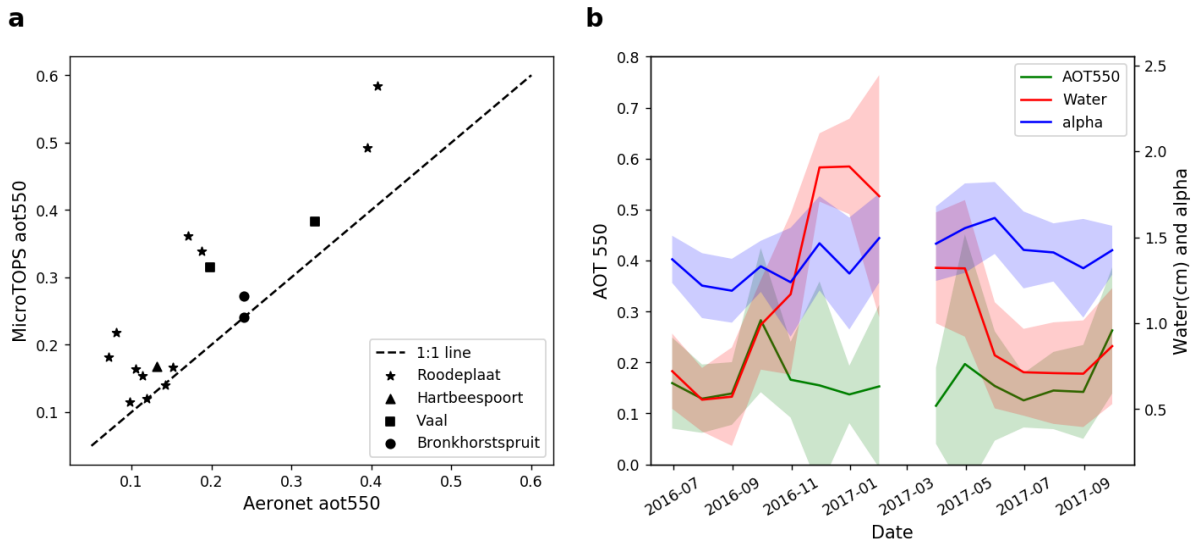

Figure 22: A) Comparison of AOT550 values from MicroTOPS and Aeronet. B) Time series of AOT 550, water vapour and alpha from the Pretoria Aeronet station coinciding the time period of field sampling campaigns.

Monthly means of AOT-550, columnar water vapour and alpha (the Angström exponent which gives an indication of particle size of the atmospheric aerosols) are given in Figure 22 B covering the period of the field campaigns. The monthly AOT-550 mean did not exhibit strong temporal or seasonal patterns and varied between 0.15 and 0.25, but large standard deviations were evident. Columnar water vapour monthly means ranged from about 0.5 to 0.7 cm during the dry season to around 2.0 cm during the wet season between November and March. The Angström exponent also did not demonstrate much seasonal variation thus indicating a rather constant aerosol particles size distribution throughout the year. The region typically experiences high amounts of biomass burning leading to increased smoke and haze in the surrounding atmosphere. Biomass burning aerosols tend to be dominated by smaller particles and a higher carbon content causing a low single scattering albedo (SSA) (Yu et al., 2013).

The analysis of variability in atmospheric properties indicates that the Highveld region of South Africa experiences large seasonal changes in water vapour content, while particle size and atmospheric load remains fairly consistent throughout the year, with unpredictable and large variability on shorter (daily or weekly) time scales. This presents a very challenging situation for systematic atmospheric correction, as it is required to account for large seasonal variability in water vapour and large short time-scale changes in atmospheric loading, characteristic of biomass burning.

3.6.3 Assessment of partial atmospheric correction

Given the very challenging problem presented by highly variable aerosol concentrations as evident from the analysis in the previous section, it is feasible to ignore aerosols when utilising certain types of algorithms. The bottom of Rayleigh (BRR) reflectance is a partial atmospheric correction that ignores effects of aerosols by correcting only for the fairly predictable Rayleigh component of scattering and absorption by air molecules (Figure 23). By normalising the spectra at 560 nm, easier comparison between the spectral shapes is facilitated, keeping in mind that Rayleigh corrected TOA reflectance will be brighter than surface reflectance by an order of magnitude difference (Figure 24).

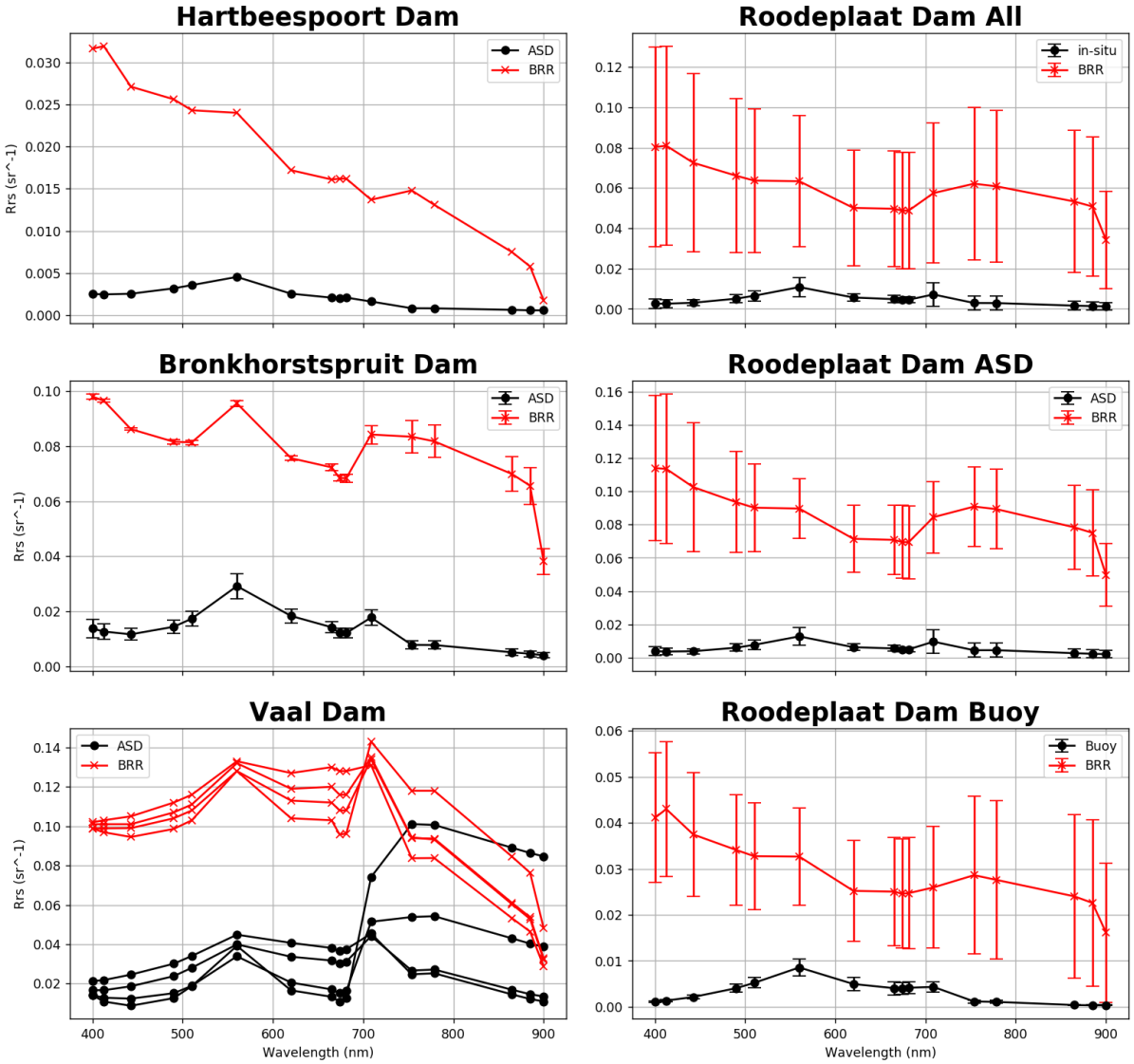

Figure 23: Comparison between BRR and in situ measured reflectance measured simultaneously.

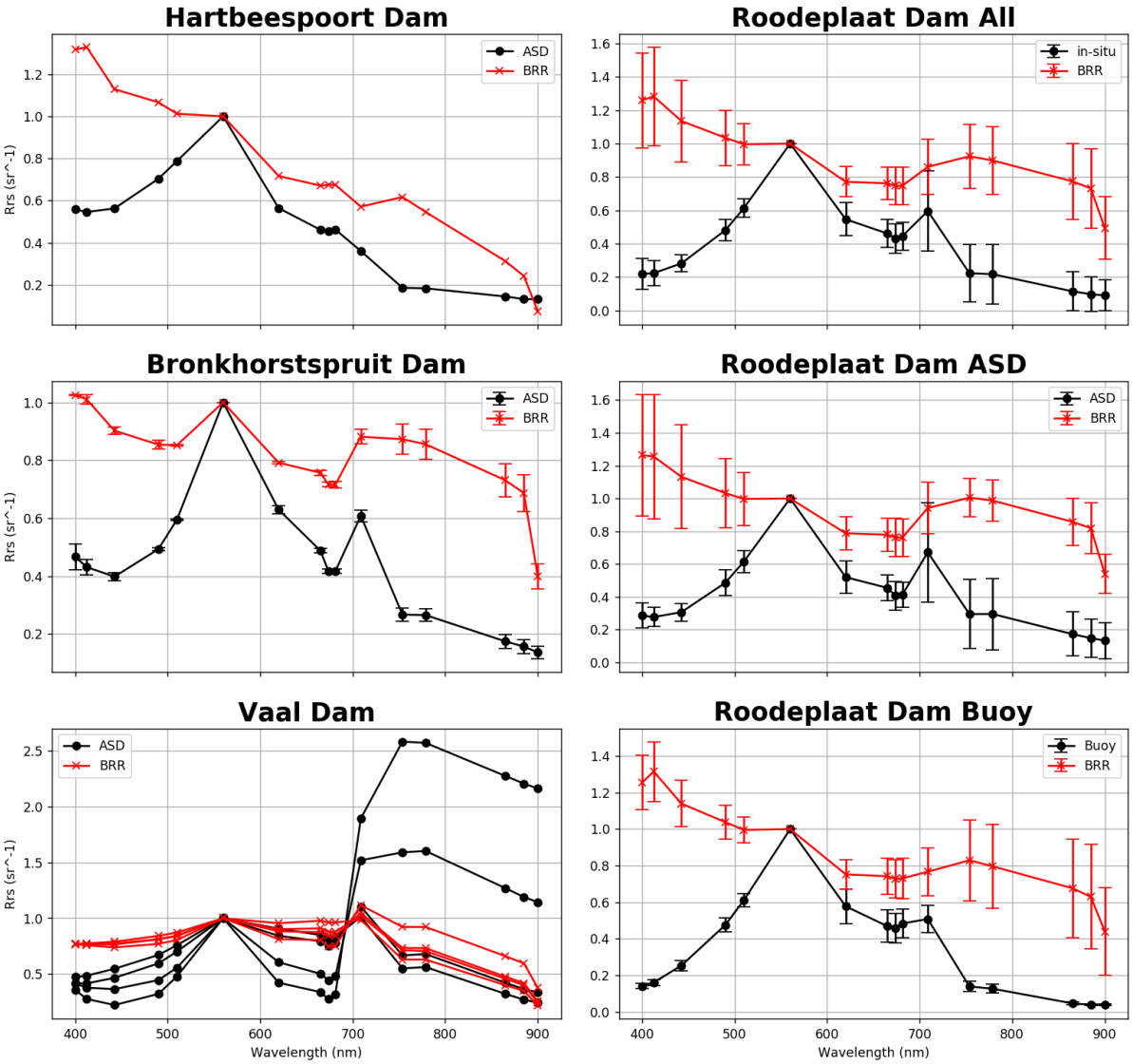

Figure 24: BRR and in situ reflectance measured simultaneously normalised at 560 nm.

It is evident that the spectral features in the region between 560 and 710 nm are very well preserved by the Rayleigh correction. The fine scale features of the bands at 560, 620, 664, 675, 681 and 709 nm are clearly visible and consistent with those measured in situ. The enlarged reflectance values in the NIR (> 700 nm) are a consequence of the adjacency effect. The loss of spectral shape also occurs in the blue where aerosols dominate the signal. However, compared to full atmospheric corrections, BRR more adequately reproduces the spectral signatures utilized by empirical band ratio approaches, leading to more accurate geophysical products as will be shown in the following section.

3.7 Assessment of chl-a retrieval algorithms with OLCI

A selection of algorithms for satellite determination of chl-a concentration were used to assess the potential of OLCI for inland water body monitoring. Traditional algorithms for Case 1 waters utilize the water leaving radiance in the blue-green part of the spectrum, however, these algorithms have been shown to perform very poorly in more turbid waters due to a breakdown of the assumption of zero water leaving radiance in the NIR due to increased contribution of non-algal particulate matter and dissolved organic material. Recent studies have shown the potential for using the red/NIR region for determination of chlorophyll concentration of higher biomass waters (Moses et al., 2009, Dall'Olmo and Gitelson, 2005, Matthews et al., 2012).

These algorithms generally utilize some sort of combination of the water leaving signal at 665, 708 and 753 nm to extract information from chlorophyll-a induced spectral features. The maximum chlorophyll index (MCI) is a chlorophyll related product that may be applied to L1b TOA data or L2. The algorithm measures the enhanced water leaving signal at 708 nm due to increased concentrations of chlorophyll and was calculated using the MCI processor within SNAP as band 11 (708 nm) relative to a baseline radiance level interpolated between either band 10 (681 nm) or band 9 (673 nm) and the upper band wavelength as band 12 (753 nm). The fluorescent line height (FLH) is a chl-a related index that can also be applied to L1b or L2 data. The FLH algorithm follows the same methodology as MCI but measures the height of the peak at 681 nm relative to a baseline between either band 8 (665 nm) or band 9 (673 nm) and band 11 (709 nm). Since OLCI L2 water products are not yet available, only L1 MCI and FLH products were used. The 2-band and 3-band models as described previously from Moses et al., 2009 were also run using the SNAP software.

The MCI, FLH, 2, and 3 band models were run on TOA radiance, TOA reflectance, and bottom-of-Rayleigh reflectance data. The MPH algorithm (Matthews et al., 2012) is a type of shifting baseline algorithm which calculates an index based on the maximum peak height between 681, 708 or 753 nm and also includes the capability of cyanobacteria detection. The MPH has already been calibrated for local waters using BRR data. This assessment uses a total of 30 match up points with coincident in-situ chlorophyll-a measurements collected on the same day as Sentinel-3A satellite overpasses between Roodeplaat, Hartbeespoort, Bronkhorstspruit, and Vaal Dams. A flowchart depicts the analysis steps in Figure 25.

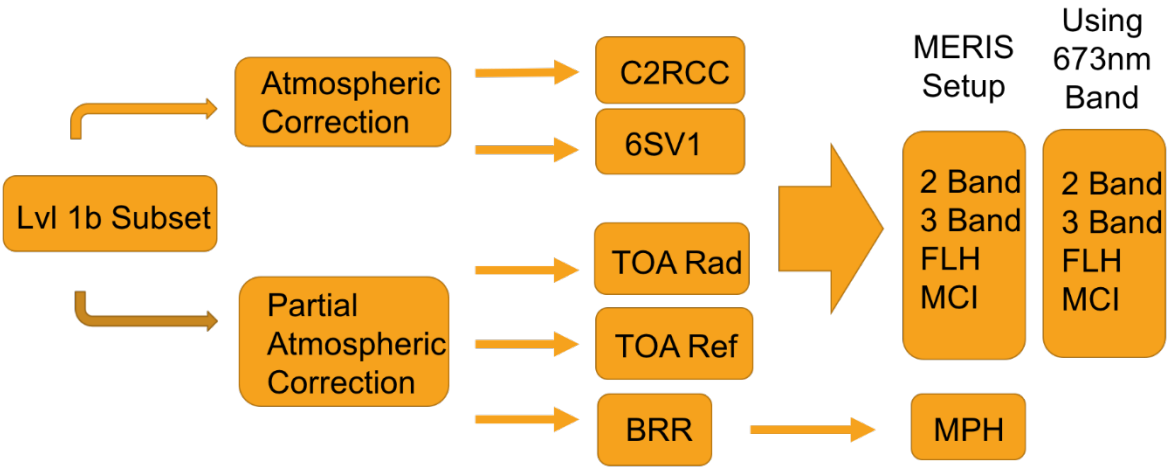

Figure 25: Flow chart depicting steps for atmospheric corrections and chl-a models.

Results from the chlorophyll-a models and in-situ measurements of chlorophyll-a are compared using basic linear regressions. Overall, the regressions were poor and the results from the linear correlations. Figure 26 displays the r-squared values for the models using top of atmosphere radiance and reflectance. The results bracketed in red are the most successful for each type of atmospheric correction. Figure 27 displays the same but for using full the atmospheric corrections, while Figure 28 displays plots for the best performing models for each stage of atmospheric correction and associated calibrated equations. From the correlation analysis, it is evident that algorithms using TOA radiance or reflectance data for chl-a estimation in this case yields better results than applying chl-a models on full atmospheric corrected data. There is little difference in the performance of the models that used TOA data.

The algorithms all had roughly the same results with r-squared values ranging between 0.3 and 0.4, the exception being the MPH algorithm with an r-squared of 0.61. The FLH algorithm generally performs better in lower biomass waters where the fluorescence peak is prominent. In higher biomass waters, or those dominated by cyanobacteria, this peak becomes overwhelmed by an increase in absorption of chl-a at 675 nm as well increased reabsorption of the fluorescent signal. This results in a trough at 675 nm and a peak at 709 nm due to the high absorption of water in the NIR (Gilerson et al., 2007; Mckee et al., 2007). This is why the best result for FLH was an inverse relationship (Figure 28A), where chl-a concentrations were correlated with deeper troughs. The better results using the MPH algorithm is most likely due to the fact that the algorithm was designed using data from South African waters and has the ability to switch essentially between an MCI or FLH type algorithm based on the spectral features of the water (Figure 28E).

Product	TOA Radiance	TOA Reflectance	BRR	n
2B665	0.414	0.425	0.344	30
2B673	0.381	0.407	0.318	30
3B665	*0.096*	0.412	0.338	30
3B673	*0.088*	0.398	0.319	30
MCI673	0.371	0.340	0.335	30
MCI681	0.394	0.384	0.368	30
FLH665	0.420	0.348	0.358	30
FLH673	0.426	0.340	0.352	30
MPHchl			0.613	23

Figure 26: Correlation coefficients from linear regressions comparing in-situ collected chlorophyll-a and model outputs using TOA radiance or reflectance. Red squares depict best performing model for each stage of atmospheric correction.

Product	6SV1	C2RCC	In-Situ	n
2B665	0.038	0.0006	0.903	30
2B673	0.100	0.0046	0.918	30
3B665	0.030	0.0035	0.923	30
3B673	0.054	0.0092	0.925	30
MCI673	0.302	0.0000	0.264	30
MCI681	0.317	0.0000	0.266	30
FLH665	0.047	0.0004	0.155	30
FLH673	0.116	0.0002	0.027	30

Figure 27: Correlation coefficients from linear regressions comparing in-situ collected chl-a and model outputs for full atmospheric corrections. Red squares depict best performing model for each stage of atmospheric correction.

When applying the chl-a models to full atmospheric corrections the results obtained were far worse than using TOA data. The massive over-correction of C2RCC, while not maintaining essential spectral features in the green and red, caused the algorithms to completely break down, evident by correlation coefficients near zero (Figure 28D). For the 6SV1 correction, while spectral features seem to have been better preserved than C2RCC, the variability in the red and NIR region of the corrected reflectance proved to contribute too much uncertainty for the models, resulting also in weak correlations (Figure 28B). The 2-band and 3-band models are designed to be applied to R_{RS} data and not necessarily TOA radiance or reflectance data. However, accurate atmospheric corrections are required to use them properly. The fact that fair performance was observed using TOA satellite data with these models is promising (Figure 28C).

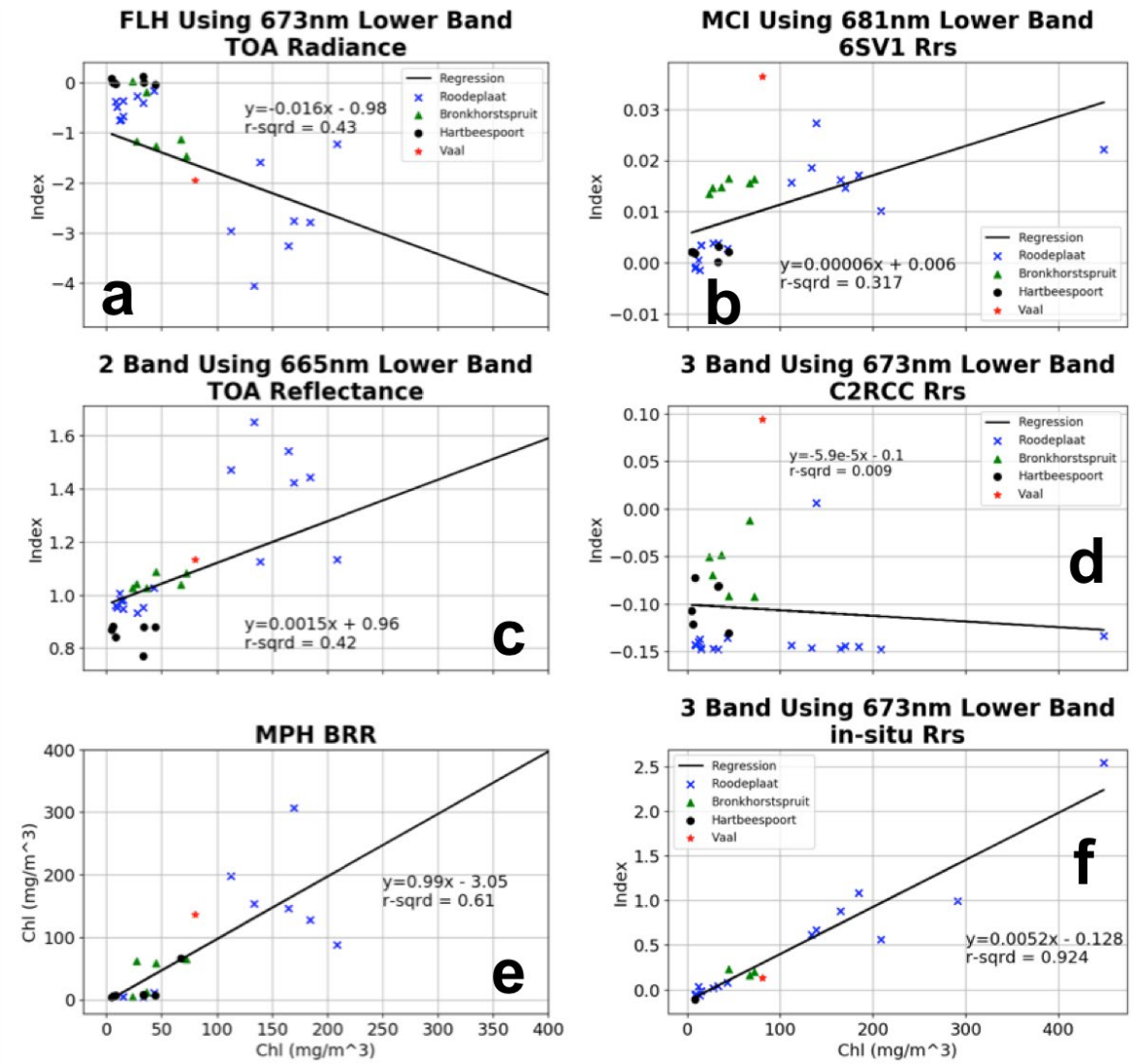

Figure 28: Plots of best performing models for each atmospheric correction stage along with calibrated equations.

When the 2 and 3-band models were applied to in-situ R_{RS}, they performed very well, with the 3-band model slightly outperforming the 2-band model (Figure 28F). The MCI and FLH algorithms do not perform well on in-situ data, again, because they are designed for two different types of waters and our dataset was too dynamic to fit into either category. The results also suggest that incorporating the new 673 nm band in the models improves the correlations coefficient slightly when using the in-situ data, while it does not seem to make much difference using the atmospherically corrected or top of atmosphere data. When using TOA data, the difference in signal between incorporating the new OLCI 673 nm band or using the MERIS band setup may not be significant enough to warrant inclusion into the algorithms.

4 CONCLUSIONS AND RECOMMENDATIONS

The success of Sentinel-3 OLCI in protecting water resources from threats such as cyanobacteria blooms and eutrophication requires high quality ground-truth data in order to assess instrument performance and properly calibrate and validate product algorithms. To accomplish this, in-situ measurements were made at four key water supply reservoirs in the Gauteng central region to obtain biogeophysical variables (chlorophyll-a, phytoplankton composition, Secchi Depth Disk, etc.) and reflectance measurements critical for validation of OLCI. Four successful field campaigns were conducted over the course of one and a half years resulting in high quality data which were used to assess the performance of OLCI radiometry and its ability to monitor small, eutrophic water targets.

In situ reference measurements indicated that the dams were eutrophic to hypertrophic and dominated by cyanobacteria, the two key risks OLCI can be used to detect and prevent. The shape and magnitude of the in-situ reference reflectance measurements were typical of waters dominated by cyanobacteria exhibiting the features typically associated with poor water quality. These targets provide ideal situation for developing methods to address these concerns and also test OLCIs capability for risk prevention. The main findings of the report are summarized below:

4.1 OLCI has outstanding radiometric quality as verified by models however the larger viewing angle presents challenges for small targets at edge of swath due to increased ground sampling distance and atmospheric path length, and reduced geolocation accuracy.

A preliminary examination of OLCI imagery indicated that a small spatial offset in the data of two to three pixels is evident in scenes with high observation zenith angles (despite correction of earlier geolocation errors). Thus, OLCI does not meet the requirement of one pixel geolocation accuracy met by MERIS after geolocation was applied. This is caused by an increase in the observation angle of OLCI relative to MERIS that was originally intended to reduce the amount of sunglint present in OLCI data. Duplication of pixels at the edge of scene pose a concern for small targets like Roodeplaat (<2 km wide) because the large viewing angle (>40º) causes pixels to be as large as 600 m. Thus, pixels with mixed signals from land and water (mixed pixels) are more prevalent and will result in poorer radiometric characterisation of the 300 m pixels.

Another consequence of an increased OZA is an increase in atmospheric path length which reduces the relative signal from the target, and could exacerbate problems from the adjacency effect. Therefore, at the edge of swath, the smallest target for which reliable radiometry can be acquired for OLCI is at least 1 800 m wide (or 3 pixels). This could reduce the number of systematic observations of small water bodies with OLCI relative to MERIS. A potential solution exists through either masking of scenes with high OZAs and applying further geo-correction to the imagery.

Despite these drawbacks associated with the changes in OZA with OLCI, the assessment of the radiometric quality at TOA provided excellent comparisons between modelled and measured data. R_{rs} was measured using the ASD and an autonomous Buoy in order to validate reflectance measurements made by the Sentinel-3 OLCI satellite instrument. The results demonstrate that OLCI provided effective characterisation of the ground target, and is a highly sensitive and well-calibrated sensor suitable for dark water targets. Its spectral performance across all visible channels was very robust. This presents excellent opportunities for systematic observation of inland waters with OLCI, unrivalled by any other sensor currently in production or in space.

4.2 The autonomous Buoy provided a high-resolution time series of high quality radiometric and geophysical measurements proving of considerable value for satellite remote sensing validation and providing unique insights into phytoplankton variability on hourly to weekly time scales.

Although no simultaneous measurements with the ASD and the Buoy were made, Rrs derived measurements using Buoy radiometry resemble high quality reflectance measurements typical of eutrophic conditions. The availability of radiometric measurements from the Buoy significantly increased the number of useable matchups compared to conventional field sampling. The successful application of common models for deriving chl-a to these radiometric measurements demonstrates the significant benefits from utilising autonomous technology for cal./val. activities. Models applied to the data allowed for continuous estimates of chl-a and other in-water parameters to be made, and this can be exploited for various applications and research areas. The high temporal resolution observations provided unique insights into the variability of phytoplankton on daily and hourly time-scales. This demonstrates how autonomous buoys can play a significant role in acquiring data for validation and calibration of algorithms used by satellite remote sensing.

4.3 The application of two atmospheric correction methods to derive water leaving reflectance from satellite measurements performed poorly. Top of atmosphere and a partial Rayleigh atmospheric correction were superior allowing application of algorithms utilising bands in the green and red spectral region.

Various types of atmospheric corrections were performed to assess best practices for using OLCI for inland water body remote sensing. Reflectance results from two fundamentally different full atmospheric corrections were compared to in-situ R_{RS} measurements The C2RCC algorithm breaks down in these types of waters most likely due to the fact that the optical properties of both the water and the atmosphere are outside of the training ranges of the algorithm. The comparative results from 6SV1 provided more accurate results in the blue and green regions of the spectrum, however, under corrected in the red and NIR over the smaller dams, most likely due to the adjacency effect. The standard error bars also show the correction is not very consistent and variable atmospheric properties can hinder successful application. This approach also requires high quality atmospheric data as input which inhibits its applicability in any operational sense.

Atmospheric data was collected during each field campaign to characterize the aerosol and water content to be used in atmospheric modelling and atmospheric corrections. The results reveal atmospheric conditions typical of biomass burning with high aerosol content and small, carbon rich, highly scattering particles. This makes proper modelling of the atmosphere for atmospheric corrections very difficult unless high quality atmospheric data is collected at the time of satellite overpass. This implicates that for inland water applications, especially in rural areas where there is typically high amounts of aerosols and biomass burning, using top of atmosphere data will for the present time yield better results.

4.4 The application of the MPH algorithm with Rayleigh corrected OLCI reflectance remains the best performing method for estimating chl-a when compared to a variety of common alternative models.

Three different stages of TOA atmospheric data were used in the assessment of various chl-a bio-optical models. Models were applied to at-sensor TOA radiance, at-sensor TOA reflectance and bottom of Rayleigh reflectance as well as reflectance output from the two full atmospheric corrections. While results were quite poor overall, they suggest applying chl-a models to TOA radiometric data yields better results. The uncertainty and error involved with applying a full atmospheric correction leads to poor comparative results. The highest performing algorithm was the MPH algorithm which was expected given it is locally tuned and

adaptability to different water types. The other algorithms performed similarly at each TOA stage. There seemed to be no advantage by incorporating the new OLCI band at 673 nm in place of the MERIS band at 665 nm in the chl-a models. However, use of the 673 nm band in models did lead to improvements when applied to in-situ R_{RS} data.

4.5 Validation of OLCI provides compelling evidence that it has the capability to provide information for protection from the twin risks of cyanobacteria blooms and eutrophication in South Africa's bulk storage surface water resources

The assessment of OLCI during instrument commissioning phase (February to July 2016) and afterwards (August 2016 to September 2017) through the acquisition of high quality datasets from an autonomous Buoy and through field measurements confirm that the sensor is optimal for monitoring small inland water bodies for the threats of cyanobacteria blooms and eutrophication, continuing the legacy of the MERIS sensor. This study has provided invaluable data for the validation, development and enhancement of existing algorithms to provide improved products from OLCI for the protection of water resources in future.

The following recommendations are made based on the findings of this research:

- Continuous development and deployment of locally-developed buoys equipped with radiometers would substantiate and add significant concomitant value to satellite-based monitoring efforts by providing high quality data for validation and development of atmospheric corrections methods, and also considerable value in short-term (daily) and long-term (monthly) monitoring of phytoplankton variability
- The MPH algorithm applied to BRR corrected data remains, according to this assessment, the most accurate method for systematic observation of chl-a from satellite remote sensing, and should be utilised in operational systems, and further developed to enhance cyanobacteria detection and chl-a estimation
- OLCI should serve as the backbone for inland water remote sensing efforts owning to its outstanding spectral and radiometric quality, and ability to apply a wide variety of geophysical retrieval algorithms
- Work should intensify to test and develop a robust atmospheric correction procedure that is applicable in inland waters where complex effects from high aerosol loading, adjacency effects (stray light) and water variability interact

5 LIST OF REFERENCES

Antoine, D., d'Ortenzio, F., Hooker, S. B., Bécu, G., Gentili, B., Tailliez, D., & Scott, A. J. (2008). Assessment of uncertainty in the ocean reflectance determined by three satellite ocean color sensors (MERIS, SeaWiFS and MODIS-A) at an offshore site in the Mediterranean Sea (BOUSSOLE project). *Journal of Geophysical Research: Oceans*, *113*(C7).

Bassani, C., Manzo, C., Braga, F., Bresciani, M., Giardino, C., & Alberotanza, L. (2015). The impact of the microphysical properties of aerosol on the atmospheric correction of hyperspectral data in coastal waters. *Atmospheric Measurement Techniques*, *8*(3), 1593-1604.

Bidigare, R. R., Marra, J., Dickey, T. D., Iturriaga, R., Baker, K. S., Smith, R. C., & Pak, H. (1990). Evidence for phytoplankton succession and chromatic adaptation in the Sargasso Sea during spring 1985. *Marine Ecology Progress Series*, 113-122.

Binding, C. E., Greenberg, T. A., & Bukata, R. P. (2011). Time series analysis of algal blooms in Lake of the Woods using the MERIS maximum chlorophyll index. *Journal of Plankton Research*, *33*(12), 1847-1852.

Birch, G. F. (2001). The clay mineralogy of sediments in the Vaal Dam and in the rivers supplying and draining the dam upstream of the barrage, *9*(3), 7530.

Bláha, L., Babica, P., & Maršálek, B. (2009). Toxins produced in cyanobacterial water blooms-toxicity and risks. *Interdisciplinary toxicology*, *2*(2), 36-41.

Brockmann, C., Doerffer, R., Peters, M., Kerstin, S., Embacher, S., & Ruescas, A. (2016, August). Evolution of the C2RCC neural network for Sentinel 2 and 3 for the retrieval of ocean colour products in normal and extreme optically complex waters. In *Living Planet Symposium* (Vol. 740, p. 54).

Byrne, M., Hill, M., Robertson, M., King, A., Katembo, N., Wilson, J., ... & Jadhav, A. (2010). Integrated management of water hyacinth in South Africa. *WRC Report*, (454/10).

Carvalho, L. R., Costa-Neves, A., Conserva, G. A., Brunetti, R. L., Hentschke, G. S., Malone, C. F., ... & Rangel, M. (2013). Biologically active compounds from cyanobacteria extracts: in vivo and in vitro aspects. *Revista Brasileira de Farmacognosia*, *23*(3), 471-480.

Chinyama, A., Ochieng, G. M., Snyman, J., & Nhapi, I. (2016). Occurrence of cyanobacteria genera in the Vaal Dam: implications for potable water production. *Water SA*, *42*(3), 415-420.

Chorus, I., & Bartram, J. (1999). Toxic cyanobacteria in water: a guide to public health significance. *World Health Organization, E&FN Spon, London*.

Cilliers, C. J. (1991). Biological control of water hyacinth, Eichhornia crassipes (Pontederiaceae), in South Africa. *Agriculture, ecosystems & environment*, *37*(1-3), 207-217.Coetzee, J. A., & Hill, M. P. (2012). The role of eutrophication in the biological control of water hyacinth, Eichhornia crassipes, in South Africa. *BioControl*, *57*(2), 247-261.

Dall'Olmo, G., & Gitelson, A. A. (2005). Effect of bio-optical parameter variability on the remote estimation of chlorophyll-a concentration in turbid productive waters: experimental results. *Applied optics*, *44*(3), 412-422.

Doerffer, R., & Schiller, H. (2007). The MERIS Case 2 water algorithm. *International Journal of Remote Sensing*, *28*(3-4), 517-535.

Downing, T. G., & Van Ginkel, C. E. (2004). *Cyanobacterial monitoring 1990-2000: Evaluation of SA data*. Water Research Commission.

Doxaran, D., Cherukuru, R. N., & Lavender, S. J. (2004). Estimation of surface reflection effects on upwelling radiance field measurements in turbid waters. *Journal of Optics A: Pure and Applied Optics*, *6*(7), 690.

DWAF (Department of Water Affairs and Forestry, South Africa) (DWAF) (2002) *National Eutrophication Monitoring Programme. Implementation Manual.* Compiled by K Murray, M du Preez and CE van Ginkel. Department of Water Affairs and Forestry, Pretoria. South Africa

Falconer, I. R., & Humpage, A. R. (2006). Cyanobacterial (blue-green algal) toxins in water supplies: Cylindrospermopsins. *Environmental toxicology*, *21*(4), 299-304.

Giardino, C., Bresciani, M., Cazzaniga, I., Schenk, K., Rieger, P., Braga, F., ... & Brando, V. E. (2014). Evaluation of multi-resolution satellite sensors for assessing water quality and bottom depth of Lake Garda. *Sensors*, *14*(12), 24116-24131.

Gilerson, A., Zhou, J., Hlaing, S., Ioannou, I., Schalles, J., Gross, B., ... & Ahmed, S. (2007). Fluorescence component in the reflectance spectra from coastal waters. Dependence on water composition. *Optics Express*, *15*(24), 15702-15721.

Gitelson, A. (1992). The peak near 700 nm on radiance spectra of algae and water: relationships of its magnitude and position with chlorophyll concentration. *International Journal of Remote Sensing*, *13*(17), 3367-3373.

Gitelson, A. A., Dall'Olmo, G., Moses, W., Rundquist, D. C., Barrow, T., Fisher, T. R., ... & Holz, J. (2008). A simple semi-analytical model for remote estimation of chlorophyll-a in turbid waters: Validation. *Remote Sensing of Environment*, *112*(9), 3582-3593.

Gitelson, A. A., Gurlin, D., Moses, W. J., & Barrow, T. (2009). A bio-optical algorithm for the remote estimation of the chlorophyll-a concentration in case 2 waters. *Environmental Research Letters*, *4*(4), 045003.

Gons, H. J. (1999). Optical teledetection of chlorophyll a in turbid inland waters. Environmental Science & Technology, 33(7), 1127-1132.

Gordon, H. R., & Ding, K. (1992). Self-shading of in-water optical instruments. *Limnology and Oceanography*, *37*(3), 491-500.

Guanter, L., Estellés, V., & Moreno, J. (2007). Spectral calibration and atmospheric correction of ultra-fine spectral and spatial resolution remote sensing data. Application to CASI-1500 data. *Remote Sensing of Environment*, *109*(1), 54-65.

Guanter, L., Ruiz-Verdú, A., Odermatt, D., Giardino, C., Simis, S., Estellés, V., ... & Moreno, J. (2010). Atmospheric correction of ENVISAT/MERIS data over inland waters: Validation for European lakes. *Remote Sensing of Environment*, *114*(3), 467-480.

Gurlin, D., Gitelson, A. A., & Moses, W. J. (2011). Remote estimation of chl-a concentration in turbid productive waters − Return to a simple two-band NIR-red model. *Remote Sensing of Environment*, *115*(12), 3479-3490.

Harding, W. R. (2015). Living with eutrophication in South Africa: a review of realities and challenges. *Transactions of the Royal Society of South Africa*, *70*(2), 155-171.

Harding, W. R., & Paxton, B. R. (2001). *Cyanobacteria in South Africa: a review*. Pretoria: Water Research Commission.

Holben, B. N., Eck, T. F., & Fraser, R. S. (1991). Temporal and spatial variability of aerosol optical depth in the Sahel region in relation to vegetation remote sensing. *International Journal of Remote Sensing*, *12*(6), 1147-1163.

Jeppesen, E., Meerhoff, M., Davidson, T. A., Trolle, D., Sondergaard, M., Lauridsen, T. L., ... & Nielsen, A. (2014). Climate change impacts on lakes: an integrated ecological perspective based on a multi-faceted approach, with special focus on shallow lakes.

Joehnk, K. D., Huisman, J. E. F., Sharples, J., Sommeijer, B. E. N., Visser, P. M., & Stroom, J. M. (2008). Summer heatwaves promote blooms of harmful cyanobacteria. *Global change biology*, *14*(3), 495-512.

Kotchenova, S. Y., Vermote, E. F., Matarrese, R., & Klemm Jr, F. J. (2006). Validation of a vector version of the 6S radiative transfer code for atmospheric correction of satellite data. Part I: Path radiance. *Applied optics*, *45*(26), 6762-6774.

Le Rouw, W. J., Schaefer, L. M., & Genthe, B. (2012). Microbial water quality in the upper Olifants River catchment: implications for health.

Martins, V. S., Barbosa, C. C. F., de Carvalho, L. A. S., Jorge, D. S. F., Lobo, F. D. L., & Novo, E. M. L. D. M. (2017). Assessment of Atmospheric Correction Methods for Sentinel-2 MSI Images Applied to Amazon Floodplain Lakes. *Remote Sensing*, *9*(4), 322.

Matthews, M. W. (2014). Distinguishing cyanobacteria from algae using bio-optical remote sensing. Phd Thesis. University of Cape Town.

Matthews, M. W., & Bernard, S. (2015). Eutrophication and cyanobacteria in South Africa's standing water bodies: A view from space. *South African journal of science*, *111*(5-6), 1-8.

Matthews, M. W., Bernard, S., & Robertson, L. (2012). An algorithm for detecting trophic status (chlorophyll-a), cyanobacterial-dominance, surface scums and floating vegetation in inland and coastal waters. *Remote Sensing of Environment*, *124*, 637-652. doi:10.1016/j.rse.2012.05.032.

Matthews, M. W., Bernard, S., & Winter, K. (2010). Remote sensing of cyanobacteria-dominant algal blooms and water quality parameters in Zeekoevlei, a small hypertrophic lake, using MERIS. *Remote Sensing of Environment*, *114*(9), 2070-2087.

McKee, D., Cunningham, A., Wright, D., & Hay, L. (2007). Potential impacts of nonalgal materials on water-leaving Sun induced chlorophyll fluorescence signals in coastal waters. *Applied optics*, *46*(31), 7720-7729.

Mishra, S., & Mishra, D. R. (2012). Normalized difference chlorophyll index: A novel model for remote estimation of chlorophyll-a concentration in turbid productive waters. *Remote Sensing of Environment*, *117*, 394-406. doi:10.1016/j.rse.2011.10.016

Mooij, W. M., Janse, J. H., Domis, L. D. S., Hülsmann, S., & Ibelings, B. W. (2007). Predicting the effect of climate change on temperate shallow lakes with the ecosystem model PCLake. *Hydrobiologia*, *584*(1), 443-454.

More, S., Pradeep Kumar, P., Gupta, P., Devara, P. C. S., & Aher, G. R. (2013). Comparison of aerosol products retrieved from AERONET, MICROTOPS and MODIS over a tropical urban city, Pune, India. *Aerosol and Air Quality Research*, *13*(1), 107-121.

Moses, W. J., Gitelson, A. A., Berdnikov, S., & Povazhnyy, V. (2009). Estimation of chlorophyll-a concentration in case II waters using MODIS and MERIS data − successes and challenges. *Environmental Research Letters*, *4*(4), 045005.

Moses, W. J., Gitelson, A. A., Berdnikov, S., & Povazhnyy, V. (2009). Satellite estimation of chlorophyll-a concentration using the red and NIR bands of MERIS − The Azov sea case study. *IEEE Geoscience and Remote Sensing Letters*, *6*(4), 845-849.

Mueller, J. L., Morel, A., Frouin, R., Davis, C., Arnone, R., Carder, K., … Voss, K. (2003). Radiometric Measurements and Data Analysis Protocols. In J. L. Mueller, G. S. Fargion, & C. R. McClain (Eds.), *Ocean Optics Protocols For Satellite Ocean Color Sensor Validation, Revision 4, Volume III:* (Vol. III, p. 78). Goddard Space Flight Space Center, Greenbelt, Maryland: NASA.

Mur, L. R., & Schreurs, H. (1995). Light as a selective factor in the distribution of phytoplankton species. *Water Science and Technology*, *32*(4), 25-34.

Nyenje, P. M., Foppen, J. W., Uhlenbrook, S., Kulabako, R., & Muwanga, A. (2010). Eutrophication and nutrient release in urban areas of sub-Saharan Africa a review. *Science of the Total Environment*, *408*(3), 447-455.

Oberholster, P. J., & Ashton, P. J. (2008). State of the nation report: An overview of the current status of water quality and eutrophication in South African rivers and reservoirs. *Parliamentary Grant Deliverable. Pretoria: Council for Scientific and Industrial Research (CSIR)*.

Oberholster, P. J., Myburgh, J. G., Govender, D., Bengis, R., & Botha, A. M. (2009). Identification of toxigenic Microcystis strains after incidents of wild animal mortalities in the Kruger National Park, South Africa. *Ecotoxicology and Environmental Safety*, *72*(4), 1177-1182.

Paerl, H. W., Hall, N. S., & Calandrino, E. S. (2011). Controlling harmful cyanobacterial blooms in a world experiencing anthropogenic and climatic-induced change. *Science of the Total Environment*, *409*(10), 1739-1745.

Palmer, K. F., & Williams, D. (1974). Optical properties of water in the near infrared. *JOSA*, *64*(8), 1107-1110.

Palmer, S. C., Kutser, T., & Hunter, P. D. (2015). Remote sensing of inland waters: Challenges, progress and future directions.

Palmer, S. C., Odermatt, D., Hunter, P. D., Brockmann, C., Presing, M., Balzter, H., & Tóth, V. R. (2015). Satellite remote sensing of phytoplankton phenology in Lake Balaton using 10years of MERIS observations. *Remote Sensing of Environment*, *158*, 441-452.

Pieterse, A. J. H., & Rohrbeck, M. A. (1990). Dominant phytoplankters and environmental variables in Roodeplaat Dam, Pretoria, South Africa. *Water SA*, *16*(4), 211-218.

Qi, L., Hu, C., Duan, H., Cannizzaro, J., & Ma, R. (2014). A novel MERIS algorithm to derive cyanobacterial phycocyanin pigment concentrations in a eutrophic lake: Theoretical basis and practical considerations. *Remote sensing of environment*, *154*, 298-317.

Robarts, R. D., & Zohary, T. (1987). Temperature effects on photosynthetic capacity, respiration, and growth rates of bloom-forming cyanobacteria. *New Zealand Journal of Marine and Freshwater Research*, *21*(3), 391-399.

Schindler, D. W., Hecky, R. E., Findlay, D. L., Stainton, M. P., Parker, B. R., Paterson, M. J., ... & Kasian, S. E. M. (2008). Eutrophication of lakes cannot be controlled by reducing nitrogen input: results of a 37-year whole-ecosystem experiment. *Proceedings of the National Academy of Sciences*, *105*(32), 11254-11258.

Simis, S. G. H., Peters, S. W. M., & Gons, H. J. (2005). Remote sensing of the cyanobacterial pigment phycocyanin in turbid inland water. *Limnology and Oceanography*, *50*(1), 237-245.

Simis, S. G. H., Ruiz-Verdu, A., Dominguez-Gomez, J. A., Pena-Martinez, R., Peters, S. W. M., & Gons, H. J. (2007). Influence of phytoplankton pigment composition on remote sensing of cyanobacterial biomass. *Remote Sensing of Environment*, *106*(4), 414-427.

Smith, V. H., Dodds, W. K., Havens, K. E., Engstrom, D. R., Paerl, H. W., Moss, B., & Likens, G. E. (2014). Comment: Cultural eutrophication of natural lakes in the United States is real and widespread. *Limnology and Oceanography*, *59*(6), 2217-2225.

Swanepoel, A., du Preez, H., Schoeman, C., Janse van Vuuren, S., & Sundram, A. (2008). Condensed laboratory methods for monitoring phytoplankton, including cyanobacteria, in South African freshwaters. *Report to the Water Research Commission BY Rand Water, 117p*.

Thirion, C. (2000). A new biomonitoring protocol to determine the ecological health of impoundments using artificial substrates. *Southern African Journal of Aquatic Sciences*, *25*(1), 123-133.

Toerien, D. F., Hyman, K. L., & Bruwer, M. J. (1975). A preliminary trophic status classification of some South African impoundments. *Water SA*, *1*(1), 15-23.

Van Ginkel, C. E. (2004). A national survey of the incidence of cyanobacterial blooms and toxin production in major impoundments. *Published by: Directorate: Resource Quality Services, Department of water Affairs and Forestry. Private Bag X313, Pretoria, 0001, South Africa*.

Van Ginkel CE. (2007). Investigating the applicability of ecological informatics modelling techniques for predicting harmful algal blooms in hypertrophic reservoirs of South Africa. PhD thesis, North-West University, Potchefstroom, South Africa.

Van Ginkel, C. E. (2011). Eutrophication: Present reality and future challenges for South Africa. *Water SA*, *37*(5), 693-701.

Van Ginkel, C. E. (2012). Algae, phytoplankton and eutrophication research and management in South Africa: past, present and future. *African journal of aquatic science*, *37*(1), 17-25.

Van Wyk, E., & Van Wilgen, B. W. (2002). The cost of water hyacinth control in South Africa: a case study of three options. *African Journal of Aquatic Science*, *27*(2), 141-149.

Vermote, E., Justice, C., Claverie, M., & Franch, B. (2016). Preliminary analysis of the performance of the Landsat 8/OLI land surface reflectance product. *Remote Sensing of Environment*, *185*, 46-56.

Vermote, E. F., & Kotchenova, S. (2008). Atmospheric correction for the monitoring of land surfaces. *Journal of Geophysical Research: Atmospheres*, *113*(D23).

Vermote, E. F., Tanré, D., Deuze, J. L., Herman, M., & Morcette, J. J. (1997). Second simulation of the satellite signal in the solar spectrum, 6S: An overview. *IEEE transactions on geoscience and remote sensing*, *35*(3), 675-686.

Walmsley, R. D. (2000). Perspectives on eutrophication of surface waters: policy/research needs in South Africa. *WRC Research Report No. KV*, *129*(00).

Walmsley, R. D., & Toerien, D. F. (1978). The chemical composition of the waters flowing into Roodeplaat Dam. *Water S. A.*, *4*(4), 192-202.

Walmsley, R. D., Toerien, D. F., & Steÿn, D. J. (1978). An introduction to the limnology of Roodeplaat Dam. *Journal of the Limnological Society of Southern Africa*, *4*(1), 35-52.

Wang, J., & Christopher, S. A. (2003). Intercomparison between satellite-derived aerosol optical thickness and PM2. 5 mass: implications for air quality studies. *Geophysical research letters*, *30*(21).

Wilson, R. T. (2013). Py6S: A Python interface to the 6S radiative transfer model. *Computers & Geosciences*, *51*(2), 166.

Yu, X., Shi, C., Ma, J., Zhu, B., Li, M., Wang, J., ... & Kang, N. (2013). Aerosol optical properties during firework, biomass burning and dust episodes in Beijing. *Atmospheric environment,* 81, 475-484.

Zohary, T. (1985). Hyperscums of the cyanobacterium Microcystis aeruginosa in a hypertrophic lake (Hartbeespoort Dam, South Africa). *Journal of Plankton Research*, *7*(3), 399-409.

APPENDIX A: TECHNOLOGY TRANSFER AND PUBLICATIONS

1. Conferences and Meetings

Sentinel-3 Validation Team (S3VT) teleconference calls hosted by Marc Bouvet (European Space Agency) and Ewa Kwiatskowska (EumetSAT). Attended by Mark Matthews, Jeremy Kravitz, Stewart Bernard. Dates of conference calls are as follows:

- 21 April 2016
- 24 May 2016
- 15 June 2016
- 11 October 2016
- 13 September 2016
- 2 November 2016
- December 2016
- 24 January 2017
- 17 February 2017
- 28 March 2017
- 26 April 2017
- 5 July 2017

Eumetsat and European Space Agency, Sentinel-3A Expert User Meeting, 28-30 June 2016, ESA-ESRIN, Frascati, Italy. Attended by: Dr. Stewart Bernard.

The 37th International Symposium on Remote Sensing of Environment, Tshwane, South Africa, 8-12 May 2017. Attended by: Mark Matthews, Jeremy Kravitz, Zimbini Faniso.

International Ocean Colour Sciences meeting, 15-18 May 2017, Lisbon, Portugal. Attended by: Mark Matthews, Jeremy Kravitz, Stewart Bernard.

European Space Agency, Commissioning review meeting, 15-17 February, 2017. Remote contributions.

2. Conference talks and posters

Matthews, M.W., 2017. Remote sensing of lakes in Africa. IOCS, Lisbon, Portugal, 15-18 May 2017. Attendance: 200+ people. Available from: http://iocs.ioccg.org/wp-content/uploads/2017/05/mon-1145-cop-matthews-web.pdf

Matthews, M.W., Kravitz, J. A., 2017. Gearing up for Sentinel-3: quantitative validation for water resources protection. Oral presentation. ISRSE 37, 8-12 May 2017, Pretoria, South Africa.

Kraivtz, J. A., Matthews, M. W., Griffith, D., 2018. Quantitative assessment of Sentinel 3 OLCI for the monitoring of small Inland water bodies in South Africa. Poster. S3VT Meeting, Darmstadt, Germany.

Kravitz, J.A., Matthews, M. W., Griffith, D., 2017. Remote sensing of inland water bodies in South Africa using Sentinel 3 OLCI. Poster. IOCS Meeting, Lisbon, Portugal.

Kravitz, J.A., Matthews, M. W., Griffith, D., 2017. Estimation of Chlorophyll-A in eutrophic inland waters using Sentinel 3 Ocean and Land Color Instrument: First Impressions. Presentation. ISRSE37, 8-12 May 2017, Pretoria, South Africa.

Faniso, Z., 2017. Determination of Aerosol Optical Properties for Retrieval of Water-Leaving Radiance at Roodeplaat Dam Relating to Calibration and Validation of Sentinel 2 and 3. ISRSE 37, 8-12 May 2017, Pretoria, South Africa.

3. Invited seminars and lectures

Jeremy Kravitz, 2017. Invited seminar: Remote Sensing of eutrophic inland systems. Council for Scientific and Industrial Research, Cape Town, South Africa.

Jeremy Kravitz, 2017. Guest Lecture: An introduction to ocean optics and remote sensing. M.Sc. Student course. University of Cape Town, South Africa.

4. Publications

Kravitz, J.A., In prep. Validation of Sentinel-3 in eutrophic inland waters. PhD Thesis. University of Cape Town.

Kravitz, J.A., Matthews, M., In prep. Validation of Sentinel-3 in small eutrophic water bodies in South Africa. Peer-review journal article.

Faniso, Z., In prep. Aerosol retrieval from Sentinel-2 and Sentinel-3. MSc Thesis. University of Fort Hare. Submitted.

5. Social media and online content

www.twitter.com/cyanolakes – reporting of project progress

Project website – http://www.cyanolakes.com/s3val/

CyanoLakes blog:

- June 4, 2016: http://www.cyanolakes.com/sentinel-3-validation/
- June 9 2016: http://www.cyanolakes.com/validation-roodeplaat-dam/
- November 11, 2016: http://www.cyanolakes.com/meet-jeremy-kravitz-phd-student/

6. Awards

Conference funding. Recipient: Jeremy Kravitz. Awardee: Eumetsat. IOCS Meeting, Lisbon, Portugal.

Conference funding. Recipient: Zimbini Faniso. Awardee: SANSA. ISRSE 37 Meeting, PTA, South Africa.

Conference funding: Recipient: Jeremy Kravitz. Awardee: SANSA. ISRSE 37 Meeting, Pretoria, South Africa.